Ref. Ares(2023)3880951 - 05/06/2023

Twin Transition for The Timber Industry

Deliverable 2.1
Input Database for Selected Wood Parts and Timber Components: Material Properties, Representative Environmental Conditions and Loads

5G-TIMBER | Work Package 2, Task 2.1

Final Delivery Date: 05-06-2023

Stefania, Fortino

This project has received funding from the European Union's Horizon Europe research and innovation programme under the Grant Agreement No 101058505.

Document Information

Project Acronym & Full Title	5G-TIMBER Secure 5G-Enabled Twin Transition for Europe's Timber Industry Sector
Project Number	101058505
Type of Action	HORIZON Innovation Actions
Topic	HORIZON-CL4-2021-TWIN-TRANSITION-01-08
Project start date/duration	01 June 2022 / 36 months
Work Package/ Result	WP2 / D2.1 Input database for selected wood parts and timber components: material properties, representative environmental conditions and loads
Result Type/ Dissemination level	DATA/ PU
Lead partner	VTT
Due date	M12
Responsible Author/Authors	Stefania Fortino (VTT) / Helena Ronkainen (VTT), Tuomas Turpeinen (VTT), Petr Hradil (VTT)
Project URL	https://5g-timber.eu/

Review Process Detail

Date	Responsible	Action
19 April 2023	Jari Halme (VTT)	Quality and Risk Manager (QRM) sends a request for the deliverable to Deliverable Responsible Person (DRP). Request is also sent to the WP Leader and the Reviewers
26 April 2023	Stefania Fortino (VTT)	DRP initially freezes the Table of Contents (ToC) in agreement with the WP Leader.
8 May 2023	Stefania Fortino (VTT)	DRP sends the draft for the named reviewers (2 or 3 persons: WP leader unless DRP & deliverable consumer(s)). Include both Word version and PDF version. PDF version is needed to check e.g., broken cross-references, fonts, layout, etc. In addition, QRM to be informed.
17 May 2023	Mari Emmus (Harmet), Aimar Parm (Hekotek) and Tord Kaasa (Jotne)	Reviewers send their reviews back to DRP for revision. QRM is also informed about the reviews
24 May 2023	Stefania Fortino (VTT)	DRP addresses the comments in one week
24 May 2023	Mari Emmus (Harmet), Aimar Parm (Hekotek) and Tord Kaasa (Jotne)	Reviewers approves the deliverable and inform Coordinator/Technical manager and QRM.
05 June 2023	Anet Tammets (TalTech)	Project Coordinator approves and saves the deliverable as the final version. Project Coordinator submits the deliverable to the European Commission.

History of changes

Version	Issue Date	% Complete	Changes	Contributor(s)
V0.1	01/03/2023	5	Initial Deliverable Structure and ToC	Stefania Fortino (VTT)
V0.2	15/03/2023	10	Initial contents for Chapter 2	Stefania Fortino (VTT)
V0.3	31/03/2023	15	Initial contents for Chapter 3	Helena Ronkainen (VTT), Tuomas Turpeinen (VTT), Petr Hradil (VTT)
V0.4	11/04/2023	20	Initial contents for Chapter 4	Helena Ronkainen (VTT), Tuomas Turpeinen (VTT), Petr Hradil (VTT)
V0.5	21/04/2023	35	Updated Chapter 2-3, added contents for Chapter 5	Helena Ronkainen (VTT), Tuomas Turpeinen (VTT), Petr Hradil (VTT)
V0.6	05/05/2023	55	Updated contents for all chapters	Helena Ronkainen (VTT), Tuomas Turpeinen (VTT), Petr Hradil (VTT)
V0.7	10/05/2023	75	Updated contents for all chapters	Helena Ronkainen (VTT), Tuomas Turpeinen (VTT), Petr Hradil (VTT)
v0.8	24/05/2023	90	Peer review	Mari Emmus (Harmet), Aimar Parm (Hekotek)
v0.9	02/06/2023	95	Updated version based on peer review comments	Stefania Fortino (VTT)
v1.0	05/06/2023	100	Quality review	Jari Halme (VTT)

V1.0	05/06/2023	100	Version for delivery	Anet Tammets (TalTech)

Disclaimer

Copyright

Table of Contents

List of Figures

List of Tables

Glossary of Terms and Abbreviations

Abbreviation / Term	Description
Ae	acoustic emission
5G	5th Generation
CLT	Cross Laminated Timber
CT	Computed Tomography
D	effective moisture diffusion
DoA	Description of Action
EU	European Union
FE	Finite Element
Fn	normal force
Ft	friction force
FSP	Fibre Saturation Point
GA	Grant Agreement
glulam	Glued Laminated Timber
GW	green wood
HTM	Hygro-Thermo-Mechanical
IoT	Internet of Things
KPI	Key Performance Indicator
L	Longitudinal

LVL	Laminated Veneer Lumber
MC	Moisture Content
MIS	Moisture Induced Stresses
PI	Performance indicator
Pd	Penetration depth
R	Radial
Rd	Residual depth
RH	Relative Humidity
SHM	Structural Health Monitoring
T	Tangential
WP	Working Package
μ	friction coefficient

1. Executive Summary

This document is the deliverable D2.1 "Input Database for Selected Wood Parts and Timber Components: Material Properties, Representative Environmental Conditions and Loads" of the Horizon Europe Innovation Action project "5G-TIMBER: Secure 5G-Enabled Twin Transition for Europe's TIMBER Industry Sector" (hereinafter also referred to as "5G-TIMBER", project reference: 101058505).

This deliverable presents the status of the work that has been carried out primarily in the task T2.1 "Development of digital material (wood) models to predict the performance of selected timber components" that runs from M2 to M24, as of M12 (May 2023) of the project.

The purpose of D2.1 is to present the input data needed for the Hygro-Thermo-Mechanical (HTM) models and the related finite element (FE) analyses planned for a follow-up deliverable, i.e., the D2.2. (Output Database for Selected Wood Parts and Timber Components: Moisture Contents and Temperatures, Moisture Induced Strains and Stresses And Crack Risk) due on M24. The data include the material properties for green wood (GW) and selected wooden components, as well as the plans to collect environmental conditions and loads to be considered in the analyses for prediction of the crack risk of timber components under moisture variations. In additions, new results of scratch tests of wood and wooden components, supported by computed tomography (CT) investigations, are collected to define a model for shear failure risk to be added to the HTM computational models, as planned in deliverable D1.1 (Descriptions of Use Cases with Expected Outcomes and Impact Projections to 3 Target Domains).

The deliverable starts with short descriptions of the mathematical models used to simulate the moisture transport in wood and the mechanical behaviour of wood material. The related properties are taken from the relevant literature and will allow to conduct HTM analyses in D2.2 for the prediction of strains and stresses with special focus on the moisture effects in wood and the related crack risk. In addition, scratch tests carried out at VTT are described, and their results are collected to provide information about the moisture effects in wood logs during cutting operations in sawmills, as well as on relevant fracture and shear properties for wooden components in sawing centres before using them to produce wooden elements of modular buildings in the production. The scratch tests are supported by CT tomography investigations and these results are also reported in the deliverable. Dataset for the results of scratch tests, in format of Excel file, are available in Zenodo at the following link: https://zenodo.org/record/7993984

The results of D2.1 support the activities previously planned in D1.1 for the initial formulation of Use Case UC1.1 (Data and Material Models Driven Lumber Production and Handling). Therefore, the reader should first familiarize with D1.1 before reading D2.1. The final computational models of D2.2 will serve as digital tools for other Tasks and Use Cases, such as the Task 2.6 about Predictive Maintenance and the Use Case UC3.2 (Long term SHM of wooden constructions: overview and requirements) about Structural Health Monitoring (SHM) of timber components.

The intended audience of public D2.1 includes all members of the 5G-TIMBER consortium, the Project Officer, and experts in the field of wood construction.

2. Introduction

Wood is a natural material widely used in the construction field as mass timber and engineered wood products [1]. Wooden components can achieve high mechanical performance not only at the material level [2], but also at the structural level. The use of wood as a sustainable building material is beneficial because of its low carbon footprint compared to other materials such as steel and concrete [3]. In spite of the numerous benefits of wood, the effects of moisture content (MC) inside the material can be a serious risk for the structural integrity and serviceability of wooden structures exposed to indoor and outdoor variable climates. The moisture gradients appearing from the exposed surfaces to the internal locations of a wooden component are due to MC changes under variable relative humidity (RH) below the fibre saturation point (FSP) of wood. Depending on the wood species, the FSP is in a MC range of 25-30%. The moisture gradients are responsible of the so-called moisture induced stresses (MIS), with consequent increase of crack risk in wooden components such as sawn timber, glued laminated timber (glulam), cross laminated timber (CLT), laminated veneer lumber (LVL), etc. [4], especially in the presence of drying.

Under favourable temperatures and MC close to the FSP, or higher, the decay due to fungi is the main problem for untreated wooden components directly exposed to the rain in outdoor conditions [5]. The biological damage of components such as decking and facades, is mainly caused by fungi ([6],[7]). Many European wood species largely used to produce building components, such as Norway spruce (*Picea abies*) and Scots pine (*Pinus sylvestris*), do not provide high durability ([8]) to biological agents and therefore need monitoring and maintenance against moisture effects.

The coating protection of wood plays a fundamental role for the maintenance of wooden components exposed to variable climates ([9]). The coating is needed to reduce the potential crack risk in the vicinity of the external wood surfaces, which increases in the presence of weak paints.

In this context, HTM numerical models can support the sensor-based monitoring as they provide a fast prediction of MC and MIS in each location of the analyzed wooden components and can quickly inform the user about the needs of maintenance activities, such as repainting, in certain periods of the year. Systems composed of embedded sensors and computational units allow further expansion of the Internet of Things (IoT) network in order to efficiently exchange the monitoring data with stationary objects in buildings. Moreover, combined with the results of the FE simulation, the whole system can provide a comprehensive understanding of the wooden components' conditions in real time.

In deliverable D2.1, the material properties needed for the HTM models are collected and an additional model for shear is also added. The results of D2.1 will be input data for deliverable D2.2 where the HTM analyses will be carried out. Later, the results of D2.2 will be inputs for deliverable D2.6 (Final 5G NPN Resource Management for Optimization of Industrial Manufacturing) about predictive maintenance.

2.1. Mapping 5G-TIMBER Outputs

This section maps the components described in the 5G-TIMBER's Description of Action (DoA)/Grant Agreement (GA), i.e., the description of the deliverable and task description in the DoA/GA, against the chapters included in this deliverable and the justification of the work conducted in the project. See Table 1.

Table 1 Adherence to 5G-TIMBER's GA Deliverable & Tasks Descriptions

5G-TIMBER GA Element	5G-TIMBER GA Element Outline	Respective Document Chapter(s)	Justification
DELIVERABLE			
D2.1 INPUT DATABASE FOR SELECTED WOOD PARTS AND TIMBER COMPONENTS: MATERIAL PROPERTIES,	DATA — DATA SETS, MICRODATA, ETC.	ALL CHAPTERS	THE CHAPTERS OF D2.1 COLLECT INPUT DATA FOR THE HTM ANALYSES TO BE PRESENTED IN DELIVERABLE 2.2, AS WELL AS NEW DATA, BASED ON SCRATCH

REPRESENTATIVE ENVIRONMENTAL CONDITIONS AND LOADS			TESTS AND CT TOMOGRAPHY OF WOOD AND WOODEN COMPONENTS FOR VALUATION OF CRACK RISK UNDER CUTTING TYPE LOADS

2.2. Deliverable Overview and Report Structure

This section describes the deliverable's structure and in particular outlines the contents of the chapters and their respective contents.

The main focus of D2.1 is the moisture effect in wood to the transportation, the installation, and the service life of wooden components.

The remaining structure of Deliverable D2.1 is organized in the following chapters:

- Chapter 3 deals with ***Models and Data Used for Hygro-thermo-mechanical Computational Models of Wood and Timber Components.*** This chapter presents the hygro-thermo-mechanical material properties needed for the HTM finite element analyses to be carried out in Deliverable D2.2.
- Chapter 4 discusses the ***Collection of New Data from Scratch Tests and X-ray Computed Microtomography of Green Wood and Timber Components.*** This chapter presents new results of scratch tests on green wood and selected wooden components, and the related CT tomography investigations. It is of great scientific relevance as the literature shows a lack of information on this issue.
- Chapter 5 presents the ***Scratch tests-based outcomes.*** Based on the results of the previous chapter, a correlation between scratch resistance and cutting resistance is found and relevant information to industrial companies are given about wood cutting operations and shear risk of wooden components under service life conditions (see Figure 1).
- *Conclusions* summarize the main topics of the D2.1 and the next steps.

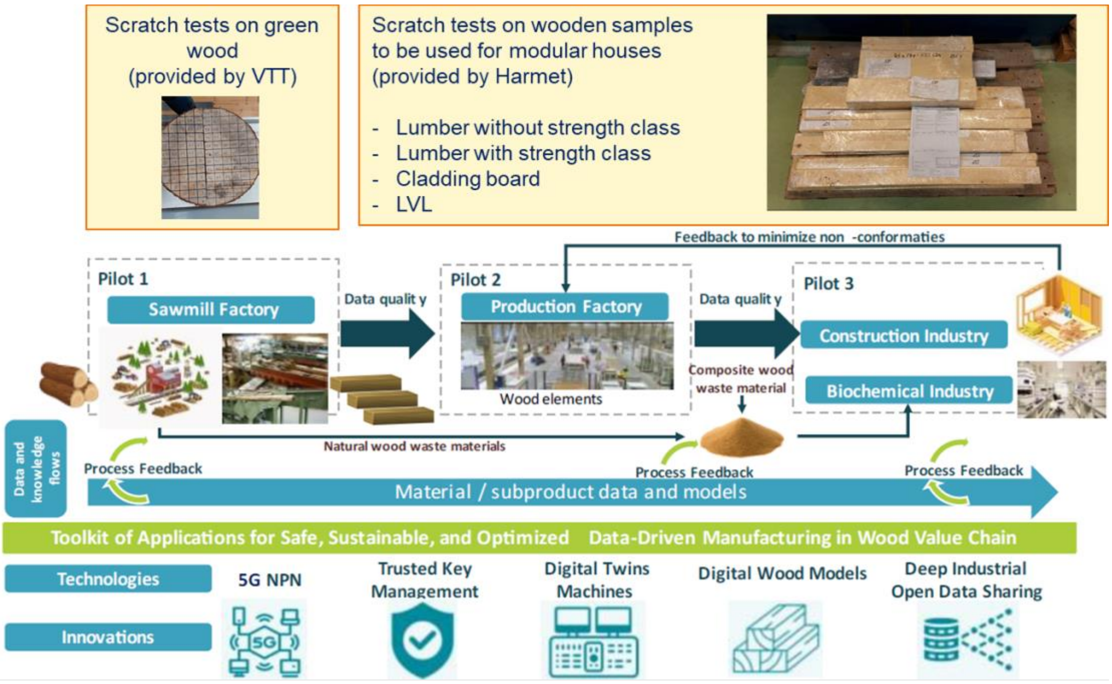

Figure 1 Scratch tests of green wood and wooden components in the context of 5G-TIMBER project. (Figure modified from the GA)

2.3 Other Project Outputs

This section describes the interdependencies with the other project tasks and activities.

a) Interdependencies between the task(s) of this deliverable and the other WPs:

D2.1 is closely connected to the activities of Use Case UC1.1 of Working Package WP1, in relation to the use of digital models for wood products with the aim to provide recommendations to sawmills, and to production and construction companies.

- For the sawmills, the impact of the moisture content on the effects of cuttings in wood is of interest. This is investigated, at the material scale, by carrying out scratch tests of green wooden samples, supported by CT tomography investigations. The measured ***scratch resistance during the scratch test*** *can be correlated to the* ***cutting resistance during the sawing process***.
- For the production and construction companies, the scratch tests, supported by CT tomography investigations, simulate, at the material scale, ***the risk of shear failure*** in selected wooden components

conditioned at different RH levels. The tests provide measures of ***fracture toughness*** and ***shear yield strength*** during cutting activities before installation or under service life loads that cause shear failure in different environmental conditions. Some example of shear failures in timber can be found in the literature (see Figures 13 and 14 in [10]).

The material properties of wood to be used in the HTM models are presented in D2.1.

b) Interdependencies between the task(s) of this deliverable and the other -same- WP Tasks

D2.1 is strictly connected to the Deliverable 2.2 (to be delivered at M24). In particular, the data collected in D2.1, i.e., the material properties of wood for the HTM computational models, will be used as input data for the FE analyses to be carried out in Task 2.2 whose results will be presented in D2.2. VTT's HTM models will numerically simulate the moisture in wood (Deliverable D2.2) and predict ***the crack risk caused by moisture induced stresses perpendicular to the grains*** in selected wooden components under variable RH.

Table 2 provides a list of the other deliverables that produce inputs to this deliverable or consume outputs from this deliverable.

Table 2 List of the other deliverables that produce inputs to this deliverable or consume outputs from this deliverable.

5G-TIMBER GA Element	Contribution and Value of linkage
D1.1 Initial descriptions of use cases with expected outcomes and impact projections to 3 target domains	**D2.1** receive instructions on the initial plans for scratch tests of wood and wooden components to be carried out at VTT in D2.1
D1.3 Initial KPIs definition report	**D2.1** receive instructions about KPIs
D2.2 Output database for selected wood parts and timber components: moisture contents and temperatures, moisture induced strains and stresses and crack risk	**D2.1** provide hygro-thermo-mechanical properties as input data for the numerical FE analyses to be presented in D2.2

3. Models and Data Used for Hygro-Thermo-Mechanical Computational Models of Wood and Timber Components

3.1. Material Properties in Moisture Transport Models for Wood

3.1.1. Short Description of the Selected Single-Fickian Model

An efficient model for moisture transport in wood was selected to present the HTM analyses in Deliverable D2.2. The method is simple to implement and has been validated and tested at VTT for the investigation of several timber components ([11], [4]). The method is based on the so-called single-Fickian theory which uses the following partial differential equation:

$$\partial c/\partial t = -\nabla \cdot \mathbf{J} \quad (1)$$

where t is the time, $c = \rho_0 MC$ is the water concentration, being ρ_0 the dry wood density and MC the moisture content of wood, and the moisture flux J is defined as

$$\mathrm{J} = -\mathbf{D} \cdot \nabla c \quad (2)$$

The moisture content 0< MC <1 is expressed as $MC = (m-m_0)/m_0$ being m the mass of the specimen and m_0 the mass of the specimen in absolute dry condition. In Equation (2), $\mathbf{D}$ represents the effective diffusion matrix of moisture transfer (**Figure 2**) which refers to both the moisture states below and above the FSP ≈ 30%. The coefficients of $\mathbf{D}$ in the various directions of wood (transverse and longitudinal) are usually named diffusivities.

The boundary condition on each exposed external surface is described by the moisture flux of Equation 3:

$$\mathrm{J}_n = \rho_0 S(MC_{eq} - MC_{surf}) \quad (3)$$

where:

- J_n = flux across the boundary

- S = surface emission or emissivity
- MC_{eq} = moisture content of wood in equilibrium with the air *RH*
- MC_{surf} = moisture content on the wood surface.

The MC_{eq} as a function of *RH* and temperature *T* of the air is called sorption isotherm. In the presence of rain, MC_{eq} = 100% is considered.

In the presence of a protective coating, the surface emission coefficient S, is given by Equation (4) where the wood surface emission S_{wood} is the material emissivity and S_{coat} the emissivity of the coating:

$$\frac{1}{S} = \frac{1}{S_{wood}} + \frac{1}{S_{coat}} \quad (4)$$

The surface emission of the coating is related to the so-called *water vapor resistance* R_{coat}. Since the emissivity units are [m/s] and the resistance units [kg/m²sPa], the transformation factor is defined as the ratio between the moisture concentration C, calculated at the testing relative humidity RH_{test}, and the related water vapour pressure P ([12]) shown in equations (5-6)

$$C = \rho_0 \, MC_{eq,\ RH_{test}} \quad (5)$$

$$P = RH_{test} \cdot e^{53.421 - \frac{6516.3}{T} - 4.125 \cdot ln(T)} \quad (6)$$

Finally, the S_{coat} is defined as

$$1/S_{coat} = R_{coat} \frac{C}{P} \quad (7)$$

3.1.2. Effective Moisture Diffusion

A short review of the effective moisture diffusion (D) parameters available in the literature for softwood materials is shown in **Table 3** and some measurements available in the literature are also presented in **Figure 2 - Figure 3**. Some of these parameters will be implemented in the HTM models to be used in D2.2.

Figure 2 shows the range of the diffusion curves, in function of the MC, adapted from [13]. Reference measurements of moisture diffusion in function of water concentration for softwood are shown in **Figure 3** from [14].

Table 3 Effective diffusion (D) parameters for single-phase models in softwood materials.

Transverse D (m2/s)	Longitudinal D (m2/s)	Ref.
measurements	measurements	[15]
based on literature (**Figure 2**)	no information	[13]
$1.5 \cdot 10^{-10}\, e^{2.28MC}$	$304 \cdot 10^{-10}\, e^{-17.7MC}$	[15]
$1.2 \cdot 10^{-10}\, e^{2.28MC}$	no information	from Toratti (1992), reference in [11]
$8.0 \cdot 10^{-11}\, e^{4.0MC}$	no information	[15]
calculations	calculations	[14], based on Siau's equations (1995)
$2.4 \cdot 10^{-10}\, e^{4.0MC}$	no information	[15]
$3.0 \cdot 10^{-10}$, 9% < MC < 16%	no information	[15]

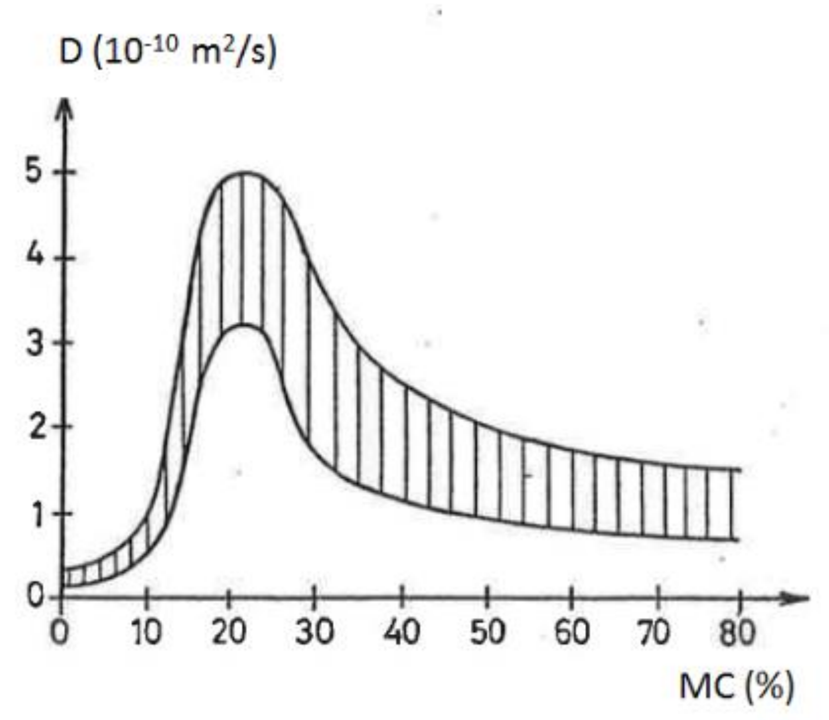

Figure 2 Range of diffusion curves in function of moisture content. Figure adapted from [13].

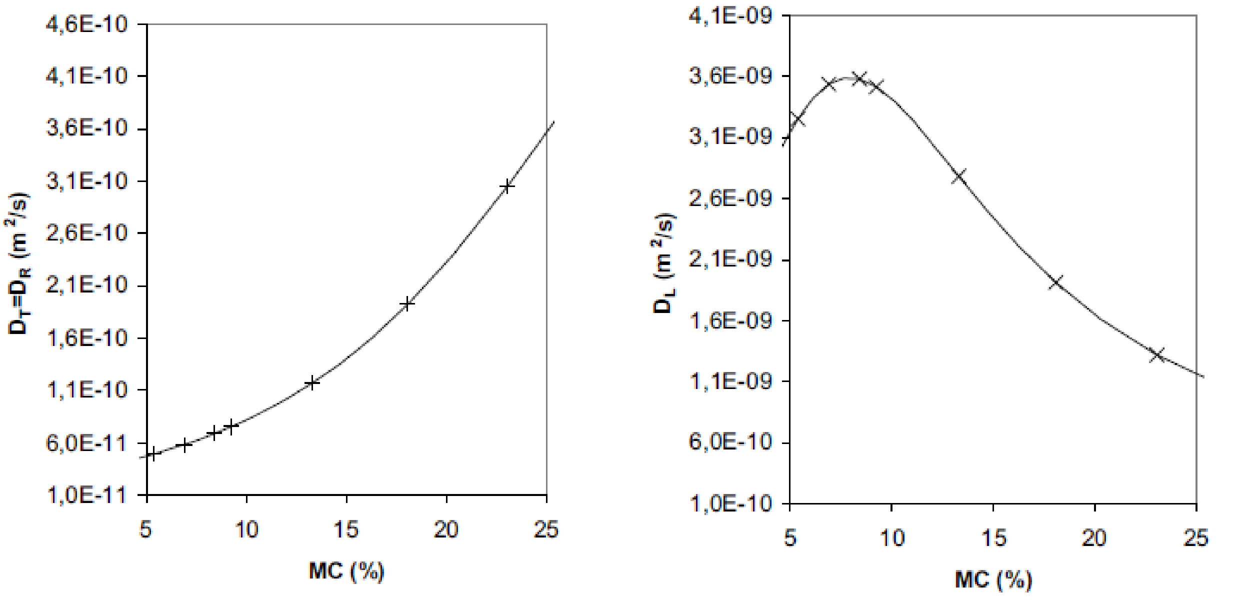

Figure 3 Diffusion curves in transversal (left) and longitudinal (right) directions of spruce wood in function of moisture content (figure adapted from [14]).

3.1.3. Sorption Isotherms

The current techniques to measure the sorption isotherms below and above the FSP are summarized in a review work [16], see Figure 4.

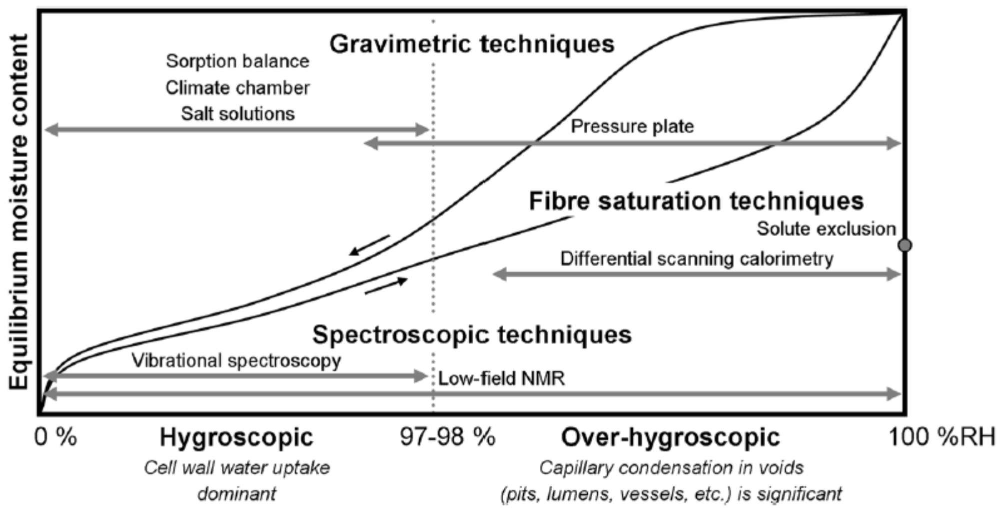

Figure 4 Schematic representation of the moisture uptake in wood during absorption from absolute dry state (lower black line) and desorption from fully water-saturated state (upper black line) in the entire RH range from dry to water-saturated. Review of techniques (gravimetric, fibre saturation, and spectroscopic) along with the covered RH range (adapted from Figure 1 of[16]).

Literature curves for the wood MC in equilibrium with the air *RH* are reported in **Figure 5, Figure 6, Figure 7, Figure 8** and **Table 4**. These curves, also called sorption isotherms, can model the sorption behaviour of wooden components, such as *massive wood and LVL*, below the FSP. For the over-hygroscopic moisture levels, that can appear in *decking components*, some measurements are available from [16](**Figure 9** and **Figure 10**). Some of the above sorption isotherms will be implemented in the HTM models to be used in D2.2.

Table 4 Sorption isotherms for softwood materials to be used in HTM numerical models.

<table>
<tr><th colspan="2">Sorption isotherms</th><th>Ref.</th></tr>
<tr><td>$$MC_{eq} = 0.01\left(\frac{-T\,ln(1-RH)}{0.13\left(1-\frac{T}{647.1}\right)^{-6.46}}\right)^{\frac{1}{110\,T^{-0.75}}}$$</td><td></td><td>[17]</td></tr>
<tr><td>Hailwood – Harrobin's model

$$MC_{eq,\alpha} = \frac{RH}{f_{1\alpha} + f_{2\alpha}RH + f_{3\alpha}RH^2}$$

$\alpha = a, d$ (adsorption, desorption)</td><td>Temperature range: +20 … +25 Celsius (Ahlgren 1972)

<table>
<tr><th></th><th>$f_{1\alpha}$ [-]</th><th>$f_{2\alpha}$ [-]</th><th>$f_{3\alpha}$ [-]</th></tr>
<tr><td>a</td><td>1.804</td><td>13.63</td><td>-12.12</td></tr>
<tr><td>d</td><td>1.886</td><td>7.884</td><td>-6.526</td></tr>
</table></td><td>Refs. in [17]</td></tr>
<tr><td>Andersson-McCharty model

$$MC_{eq,\alpha} = -\frac{\ln\left(\ln(1/h)/f_{1\alpha}\right)}{f_{2\alpha}}$$

$$f_{i\alpha} = \sum_{j=0}^{n} b_{ij}^{\alpha} T^j,\ i \in \{1,2\}$$

$\alpha = a, d$ (adsorption, desorption)</td><td>Temperature range: 5… +25 Celsius (from review in [17], paper 6)

<table>
<tr><th>Species</th><th>α</th><th>n</th><th>b_{12}^{α} [K^{-2}]</th><th>b_{11}^{α} [K^{-1}]</th><th>b_{10}^{α}</th><th>b_{22}^{α} [K^{-2}]</th><th>b_{21}^{α} [K^{-1}]</th><th>b_{20}^{α}</th></tr>
<tr><td>?</td><td>?</td><td>1</td><td>0</td><td>−0.0143</td><td>7.73</td><td>0</td><td>0.0567</td><td>0.875</td></tr>
<tr><td>sitka spruce</td><td>d</td><td>2</td><td>-4.228×10^{-5}</td><td>0.0196</td><td>1.47</td><td>9.53×10^{-4}</td><td>−0.518</td><td>87.6</td></tr>
<tr><td>klinki pine</td><td>a</td><td>1</td><td>0</td><td>−0.0234</td><td>11.1</td><td>0</td><td>0.0657</td><td>0.0865</td></tr>
<tr><td>klinki pine</td><td>d</td><td>1</td><td>0</td><td>−0.0367</td><td>16.3</td><td>0</td><td>0.0535</td><td>2.13</td></tr>
</table>

Temperature range: -25 … +30 Celsius (fitted in [9] from measurements from Hedlin, 1967)

<table>
<tr><th>α</th><th>n</th><th>b_{10}^{α} [-]</th><th>b_{11}^{α} [K^{-1}]</th><th>b_{20}^{α} [-]</th><th>b_{21}^{α} [K^{-1}]</th></tr>
<tr><td>a</td><td>1</td><td>7.719</td><td>-0.011</td><td>5.079</td><td>0.046</td></tr>
<tr><td>d</td><td>1</td><td>9.739</td><td>-0.017</td><td>-13.419</td><td>0.100</td></tr>
</table></td><td>Refs. in [17] and [18]</td></tr>
</table>

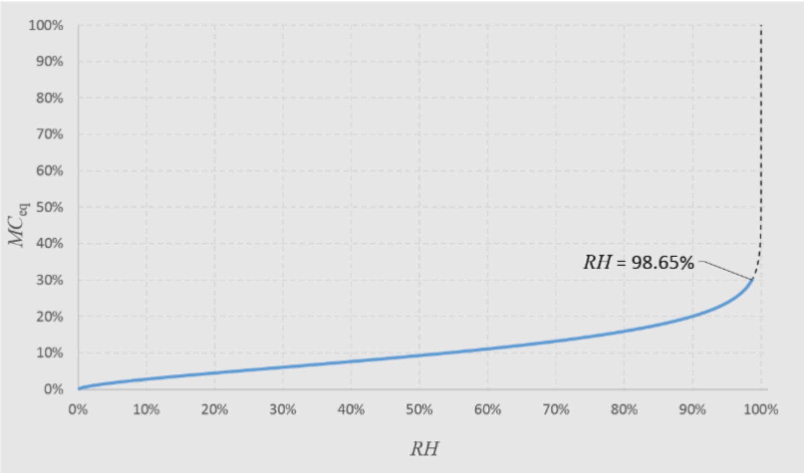

Figure 5 Sorption isotherm from [19] used for softwood moisture calculations in the literature. In black dashed line the part of the curve affecting the moisture state above the FSP (MC=30%).

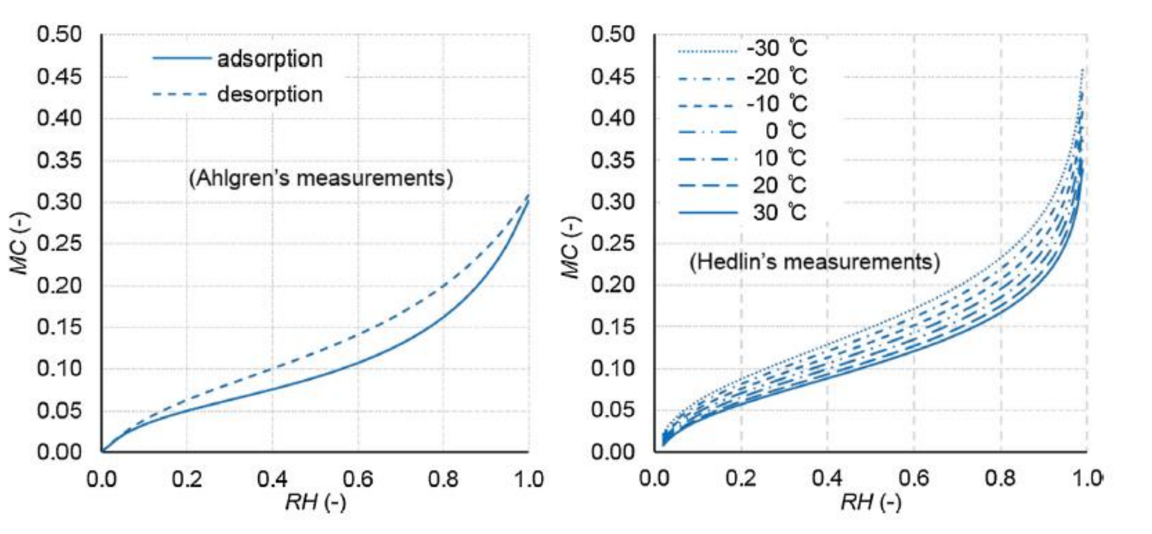

Figure 6 Left: Hailwood – Harrobin adsorption and desorption curves fitted on Ahlgren´s measurements for spruce wood at T=23 ℃ (reference in [17]*). Right: Anderson-McCarty average sorption curves at different temperatures extrapolated from Hedlin´s measurements for softwood (interpolated in* [9]*).*

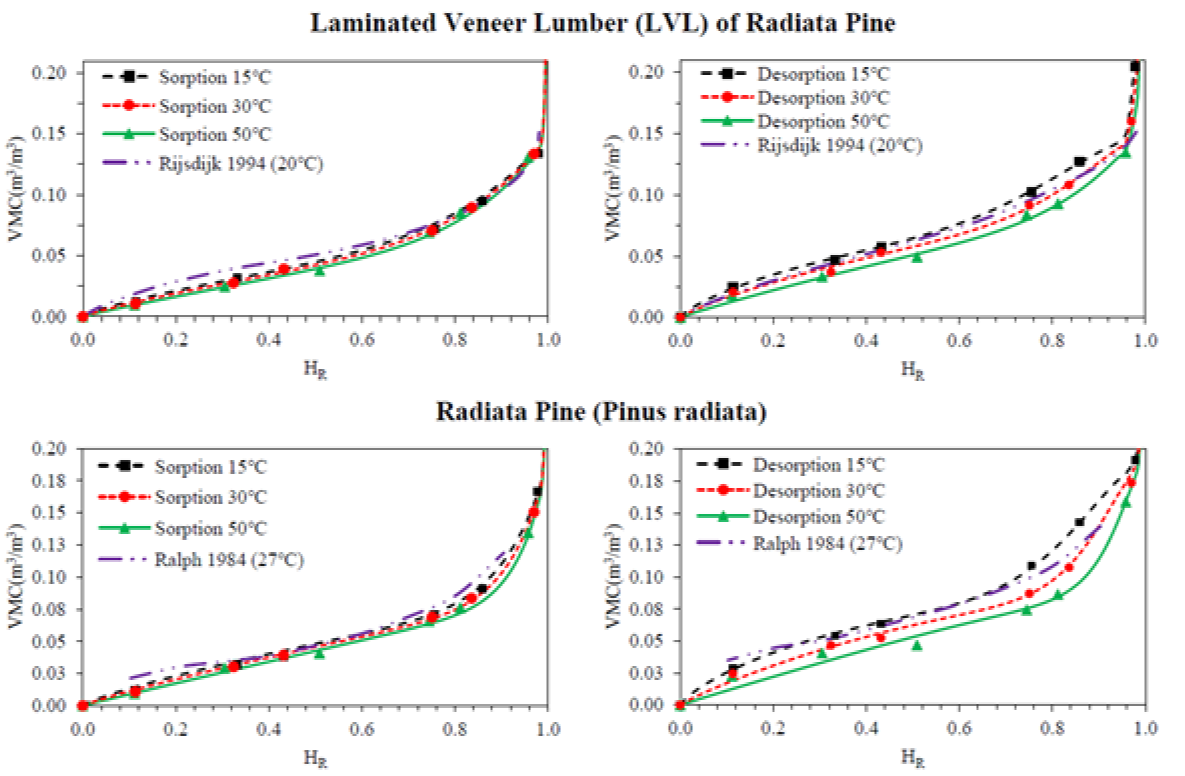

Figure 7 Sorption (adsorption) and desorption isotherms for LVL of Radiata Pine (Top) and of Radiata Pine (Bottom) at different temperatures. Figure adapted from [20].

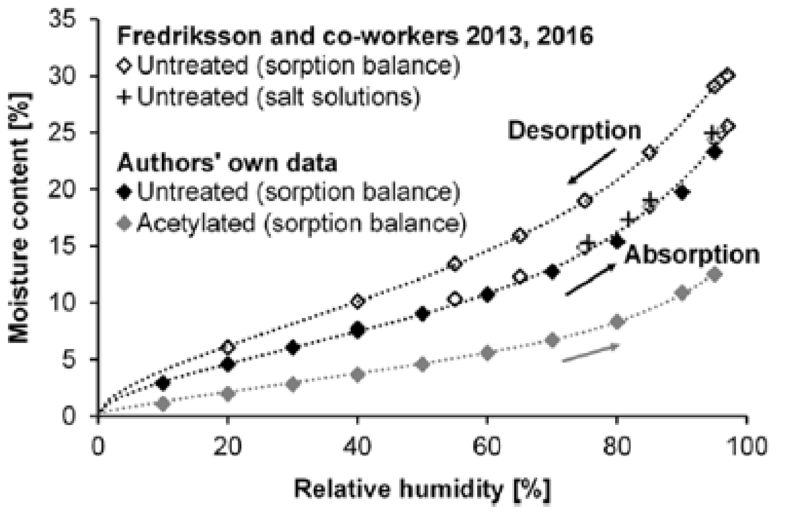

Figure 8 Sorption isotherms for desorption from water-saturated state and absorption from dry state for untreated and acetylated Norway spruce in the range of 0–97% (RH). (Adapted from Figure 2 of [16]*).*

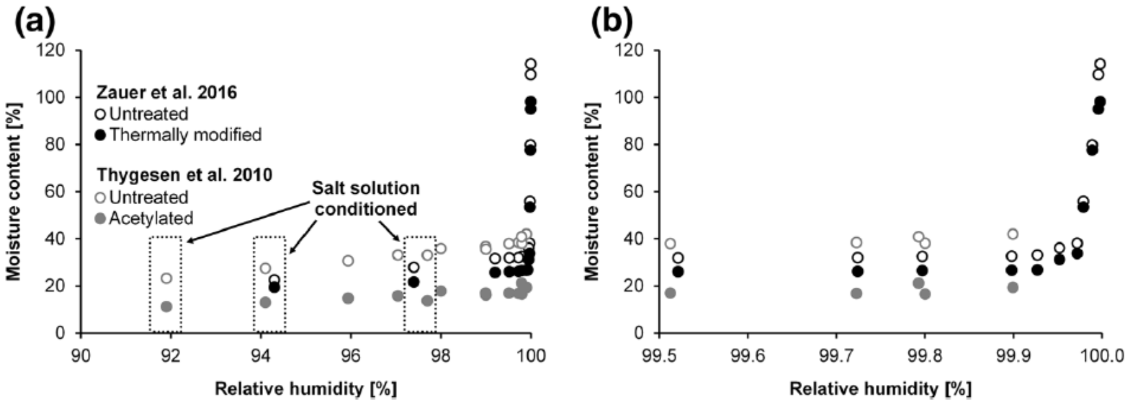

Figure 9 (a) Desorption isotherms in the over-hygroscopic range determined after conditioning with the pressure plate technique and saturated salt solutions for untreated and modified Norway spruce. (b) Zoom of (a) in the 99.5–100.0% RH range (adapted from Figure 3 of [16]).

3.1.4. Surface Emission of Wood and Protective Coatings

The values of surface emission for wood available in the literature span in a range of $1e^{-8}$ - $2e^{-7}$ [m/s] (see references in [11]).

To measure the surface emission in the presence of a paint, the testing of relative humidity depends on the method used to measure the water vapour resistance. Common methods are the dry cup and the wet cup that are also adopted within the standard [21]. In many dry cup measurements, the relative humidity is around 90% [22]. The water vapour resistance of paints depends on the ambient relative humidity as well as on the MC of the substrate.

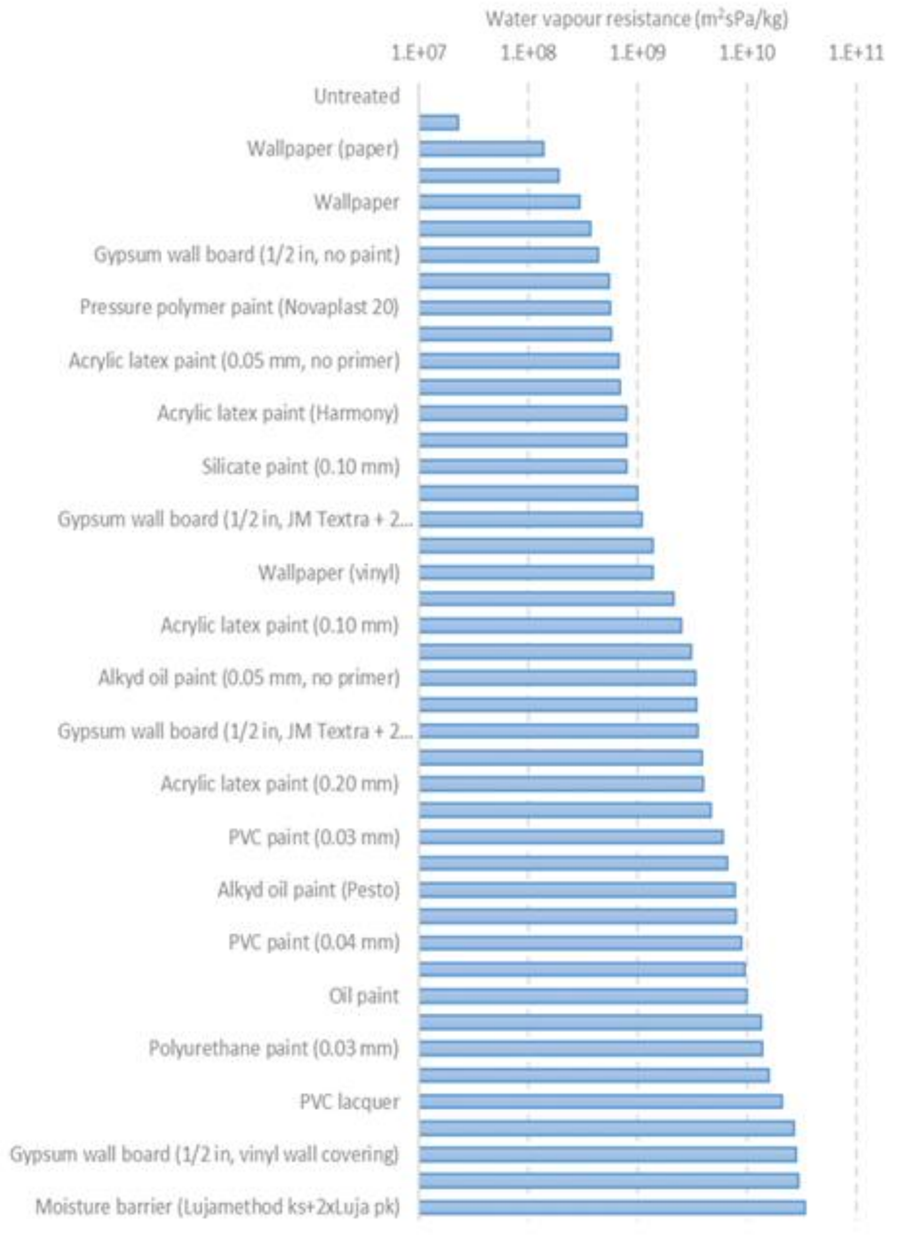

Figure 10 Values of water vapour resistance in various coatings (from [22]).

It should be noticed that the permeances (i.e., the inverse of the water vapour resistances), measured with the method of the wet cup, are usually 3-5 times higher than those measured by the dry cup method. Some values of water resistance for different coatings are shown in Figure 10 and the details are listed in Appendix I.

To transform the water vapour resistance permeance in surface emission coefficient for the numerical models, Equation (7) should be used.

3.2. Material Properties in Mechanical Models for Wood

3.2.1. Short Description of the Selected Orthotropic-viscoelastic mechanosorptive Model

The calculation of moisture induced stresses (MIS), which will be presented in the HTM models of Deliverable D2.2, is based on the orthotropic-viscoelastic-mechanosorptive material model by [11]. A short summary is presented below.

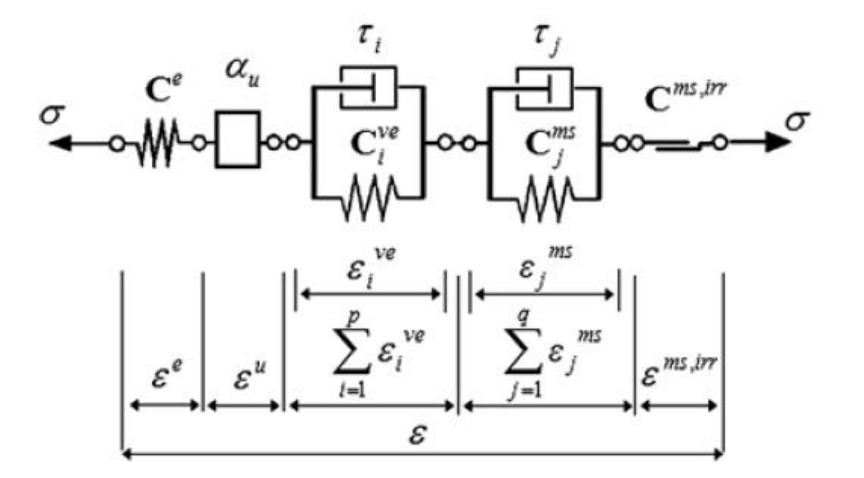

Figure 11 Scheme of the constitutive model for wood ([11]).

The model consists in five deformation mechanisms in series that provide a decomposition of strain into elastic deformation, hygroexpansion, viscoelastic creep, recoverable mechanosorption and mechanosorptive irrecoverable creep (Figure 11). The elastic strain matrix of the model is defined as

$$\boldsymbol{\varepsilon}^{\mathrm{e}} = \boldsymbol{\varepsilon} - \boldsymbol{\varepsilon}^{\mathrm{MC}} - \sum_{\mathrm{i}=1}^{p} \boldsymbol{\varepsilon}_{\mathrm{i}}^{\mathrm{ve}} - \sum_{\mathrm{j}=1}^{q} \boldsymbol{\varepsilon}_{\mathrm{j}}^{\mathrm{ms}} - \boldsymbol{\varepsilon}^{\mathrm{ms,irr}} \qquad (8)$$

where:

- $\boldsymbol{\varepsilon}$ = total strain;
- $\boldsymbol{\varepsilon}^{\mathrm{MC}}$ = hygroexpansion strain;
- $\boldsymbol{\varepsilon}_{\mathrm{i}}^{\mathrm{ve}}$ = viscoelastic elemental creep strains and p = number of viscoelastic elements;
- $\boldsymbol{\varepsilon}_{\mathrm{j}}^{\mathrm{ms}}$ = mechanosorptive elemental creep strains and q = number of mechanosorptive elements;
- $\boldsymbol{\varepsilon}^{\mathrm{ms,irr}}$ = irrecoverable mechanosorptive strain.

For the derivation of all stresses and strains and the elemental matrices of the model, the reader is referred to ([11]), where the constitutive model was validated with respect to experimental results relative to small scale wood specimens ([23]) and small glulam sections ([24]) under mechanical loading in both cases of constant and variable humidity conditions.

3.2.2. Mechanical Properties

Referring to the radial (R), tangential (T) and longitudinal (L) wood directions, some of the elastic parameters adopted in the literature for wood, which is an anisotropic material, often modelled as orthotropic, are listed in **Table 5**.

Table 5 Elastic parameters used in Abaqus code for HTM models of softwood

E_{R} (MPa)	E_{T} (MPa)	E_L (MPa)	G_{RT} (MPa)	G_{RL} (MPa)	G_{TL} (MPa)	ν_{RT} (-)	ν_{RL} (-)	ν_{TL} (-)	Ref.
900	600	13500	40	700	700	0.558	0.038	0.015	[18]
817	420	11900	42.5	743	624	0.555	0.038	0.014	[24]

with:

- E_{R}, E_{T}, E_L: elastic moduli in the orthotropic directions of the local coordinate system with directions;
- G_{RT}, G_{RL}, G_{TL}: shear moduli in the orthotropic planes RT, RL and TL;
- ν_{RT}, ν_{RL}, ν_{TL}: Poisson's ratios.

The hygroexpansion parameters, as well as the viscoelastic and mechanosorptive creep parameters adopted for the HTM analyses, will be taken from ([11]).

3.3. Representative Environmental Conditions and Loads

3.3.1. Weather Loads in Indoor Conditions

The two reference buildings where indoor conditions will be observed, are located in Finland, in the cities of Rovaniemi and Sipoo. Both buildings are kindergartens made of wooden modules and the data about the indoor climate information (at least information about temperature and RH) is received via low power cellular IoT-based sensors installed into these buildings.

3.3.2. Weather Loads in Outdoor Conditions

The outdoor climates needed for the HTM analyses will be extracted from the Finnish Meteorological Institute website https://en.ilmatieteenlaitos.fi/

The raw data are handled by using the VTT HYGRO tool implemented in the VTT Modelling Factory environment in previous VTT projects: https://modellingfactory.org/content/hygro.

The weather of Sipoo zone is not directly available and therefore, the data of the close city of Vantaa are used.

As an example, 1 year-reference weather data for Rovaniemi and Sipoo (from 15.3.2022 to 14.3. 2023) are shown in **Figure 12** and **Figure 13** in terms of relative humidity, temperature and millimeters of rain. The correct weather data will be defined later for the analyses to be presented in D2.2.

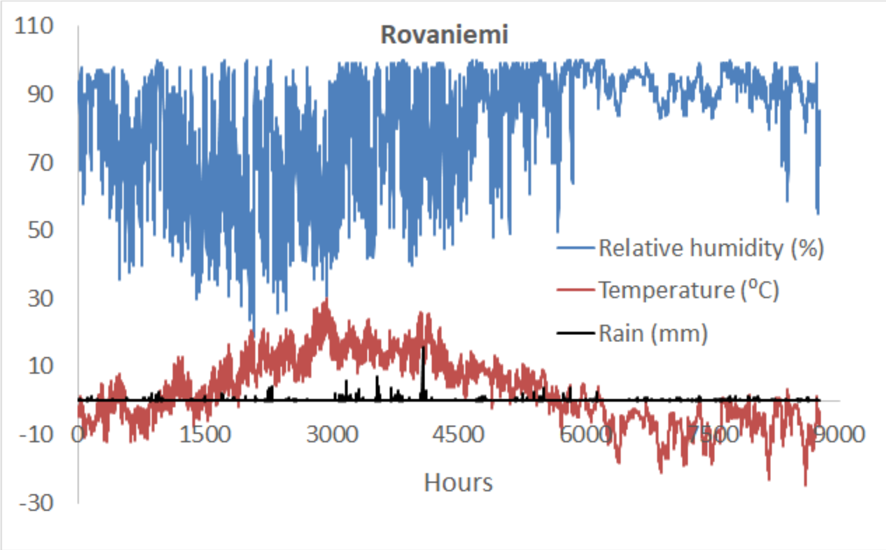

Figure 12 Outdoor weather in Rovaniemi during 8760 hours from 15.3.2022 to 14.3.2023.

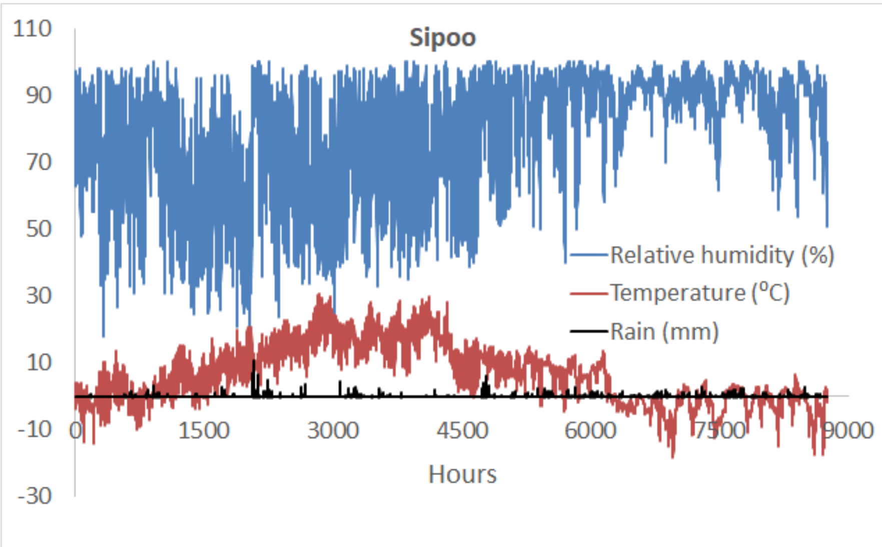

Figure 13 Outdoor weather in Sipoo during 8760 hours from 15.3.2022 to 14.3.2023.

4. Collection of New Data from Scratch Tests and X-ray Computed Microtomography of Green Wood and Timber Components

4.1. General Description of Scratch Tests

In the scratch test, an indenter is loaded against the sample surface while the sample is moved in a controlled way, which generates a scratch channel on the sample surface. Figure 15c shows a sample of scratch test being made. Scratch test can be used for micro-abrasion and scratch resistance testing as well as for the adhesion evaluation of surface coatings.

The scratch tests of different wood samples (see sections 4.1.1. and 4.1.2) are carried out at VTT with a Micro-Combi Tester by CSM Instruments. A Rockwell C indenter with a diamond tip with radius of 200 μm was used for scratching. The scratch tests were conducted as follow:

- The tests are carried out in the controlled laboratory environment having 50 ± 5 % RH and 21 ± 1 °C temperature.
- The load is applied in a constant mode using three normal load levels, namely 4 N, 10 N, and 20 N. The scratch length was 10 mm and the scratching speed 10 mm/min.
- During scratch testing the following measurements are carried out:
  - normal force Fn (i.e., the indenter force);
  - friction force Ft (i.e., the scratch resistance of wood resisting to the scratch movement);
  - acoustic emission Ae;
  - penetration depth Pd (i.e., the sum of elastic and plastic deformation of the sample material during scratch test).
- In addition, after the tests, the following measurements are collected:
  - residual depth Rd (i.e., the remaining plastic deformation of the material);
  - friction coefficient μ (i.e., the scratch resistance divided by the normal force, which describes the resistance to scratch action).

The same approach was used in previous research for scratch tests of green wood carried out by some of the authors in ([25]).

4.1.1. Scratch Tests of Green Wood

This work was carried out in collaboration with the Academy of Finland project WaterInWood (Decision number 349194) in which VTT acts as the coordinator and partners are Luke (Natural Resources Institute Finland) and University of Jyväksylä. The green wood (GW) samples of pine (*Pinus sylvestris*) were prepared from a 40 mm thick cross section of pine wood delivered to VTT from Luke after the tree was cut in the forest. This cross section was cut into small 20 mm x 20 mm x 30 mm samples (Figure 14).

Altogether there were 99 samples and the samples from no 44 to no 69 were selected for the scratch tests, since they provided a good representation of different areas of the wood cross section.

The samples were stored in the controlled laboratory environment prior to tests (50 ± 5 % Rh, 21 ± 1 °C).

(a) (b)

Figure 14 (a) The cross section of the pine wood and (b) the samples cut from the cross section. The samples selected for the scratch tests are no 44 to no 69.

The scratches were made on three sides on the wood samples in three directions. The scratch directions of sample no 75 are presented in Figure 15, where the R refers to radial direction, T to tangential direction, and L to longitudinal direction. **Figure 16** represents as an example the scratch resistance (Ft), friction coefficient (μ), penetration depth (Pd), and residual depth (Rd) graphs from the scratch tests carried out on the sample no 67.

Figure 15 (a) and (b) The scratch directions R, T and L of the wood sample. (c) The test sample in the Micro-Combi tester positioned for scratch testing.

(a) (b) (c)

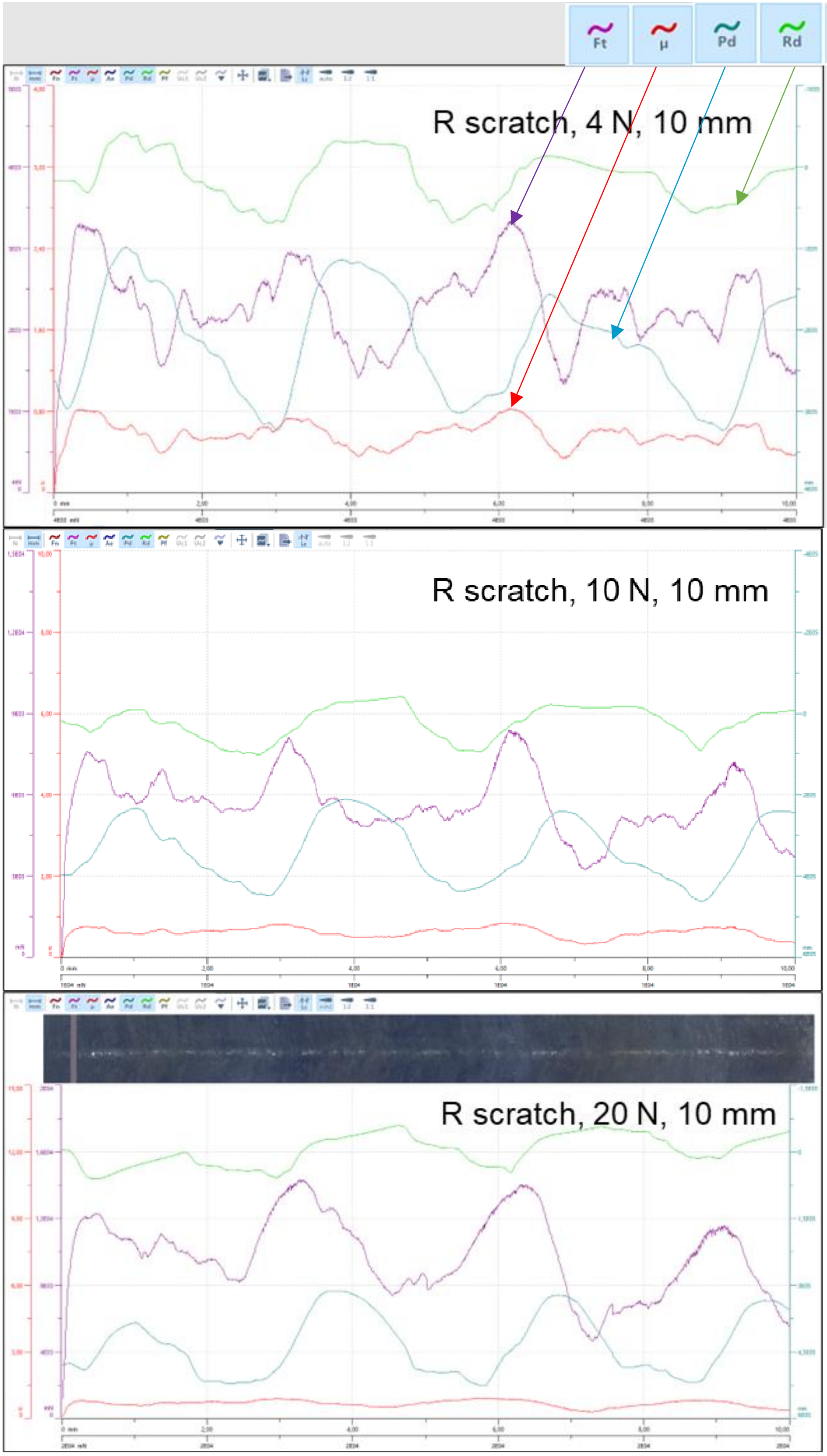

Figure 16 The scratch resistance (Ft), friction coefficient (μ), penetration depth (Pd), and residual depth (Rd) of sample no 67 from tests with normal load of (a) 4 N, (b) 10 N, and (c) 20 N.

4.1.2. Scratch Test of Timber Components

The timber components received from partner Harmet and selected for the scratch tests are listed in **Table 6**. Two components represented the timber with strength glass C24 (no 1 and no 2) and two without strength classification (no 7 and no 10). Components no 1 and no 7 were classified as "not good ones" as they show some damages. Two samples were laminated timber components and one (14) cladded board.

The timber components were cut into small size samples of 20 mm x 20 mm x 30 mm for the scratch tests (**Figure 17**). The samples were kept in the humidity cabins with 65 % and 85 % humidity, to expose the materials at different humidity levels and thus provide information on the effect of humidity on the timber performance. The density of the components listed in the table was determined to represent the density in the stabilised humidity conditions. The scratch tests were carried out immediately after removing from the cabin to retain the humidity of the samples. The similar scratch test procedure presented above for the green wood was applied also for these timber samples.

Table 6 The timber components selected for scratch testing. The density of samples was determined after storage in 65 % and 85 % humidity.

Code	Sample	Size (mm)	Length (m)	OK/NOT	Date of packing	MC before packing (%)	Treatment	Density at RH 65% (kg/m3)	Density at RH 85% (kg/m3)
1	Timber sample with strength class C24	45×120	2×0.55	NOT	12.1.2023	12	no	476	491
2	Timber sample with strength class C24	45×170	2×0.53	OK	12.1.2023	10	no	389	396
7	Timber sample without strength class	28×70	2×1.0	NOT	12.1.2023	10	no	443	471
10	Timber sample without strength class	28×95	1.0	OK	12.1.2023	10	no	417	420
5	Kerto LVL, S-Beam	45×120	1.0	OK	12.1.2023	9	no	509	476
9	Kerto LVL, T-Stud	45×95	1.0	OK	12.1.2023	11	no	431	464
14(H)	Cladding board/Timber	18×121	0.91+0.73	OK	12.1.2023	10	no	462	438

	sample without strength class								
14(M)	Cladding board/Timber sample without strength class	18×121	0.91+ 0.73	OK	12.1.2023	10	Acrylic water dispersion paint	439	437

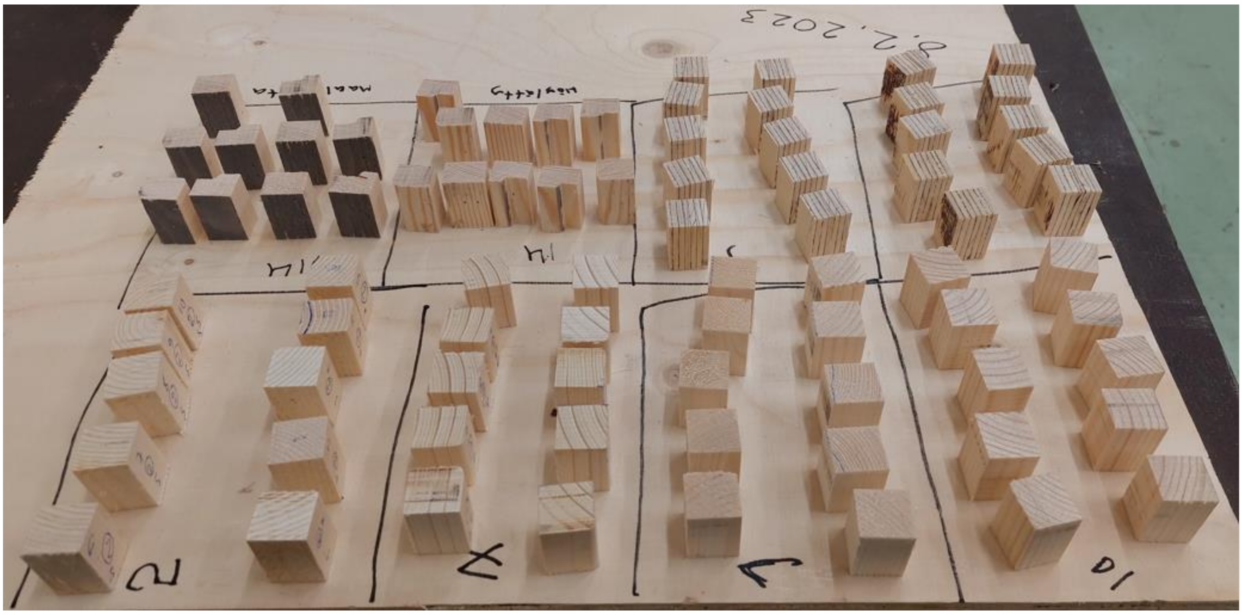

Figure 17 The 20 mm x 20 mm x 30 mm samples cut from the timber components for tests.

4.2. X-ray Computed Tomography

4.2.1. X-ray Computed Tomography for Green Wood Samples

The tomography work for green wood samples was carried out at University of Jyväskylä within the collaboration of 5G-TIMBER project with the Academy of Finland project WaterInWood, coordinated by VTT. Since the CT device of University of Jyväskylä allows a higher accuracy than the one available at VTT, the work was aimed to identify the deformation mechanisms of wood cell walls under the scratches. This is important to justify the correlation between scratch mechanisms at the material scale and cutting mechanisms at the macroscale.

A reference sample, the nr. 75 in **Figure 15**, was tested to assess a methodology of tomography investigation for scratched wood. Three wood samples (12 mm × 3 mm × 3 mm) were cut from the original wood sample such that each sample contained all the three scratches (scratching force 4 N, 10 N and 20 N) of either longitudinal, radial or tangential direction.

Each sample was glued from the ends to a half-cylindrical part of a carbon fibre rod (diameter 3 mm) such that the surface containing the scratches was against the flat surface of the rod. The rods and the samples were then ground with a high-speed grinding tool to a diameter of 1.8 mm.

The scratches were scanned at University of Jyväskylä with an Xradia MicroXCT-400 microtomography device using 40 kV tube voltage and 100 μA tube current without filtering (resolution ranging from < 100 nm to tens of μm). A total of 1505 projection images of size 2000 px × 2000 px were taken with an exposure time of 7 s and a pixel size of 1.1 μm. As only one scratch fitted in the field of view (2.2 mm × 2.2 mm) at a time, each sample was scanned three times (Figure 18). The total scanning time of a single scan was around 8 h, and all the scans around 72 h. All the scans were reconstructed to produce three-dimensional tomographic images of size 2000^3 voxels with a voxel size of 1.1 μm. The tomographic images show the wood cell mechanisms under the scratches, as it is discussed in the results section.

In addition, the tomographic images were used to measure the average dimensions of the scratches. The three-dimensional images were first averaged along the scratch to obtain a two-dimensional image, from which the average cross-sectional area and the depth of the scratch were estimated (average over 2 mm length). As the cross-sectional shapes of the scratches resembled Gaussian curves, the width of a scratch cannot be determined directly. Instead of this, the average width was calculated using the cross-sectional area and the depth of the scratch. It also seems that the results depend on the wood structure (earlywood or latewood) being scratched.

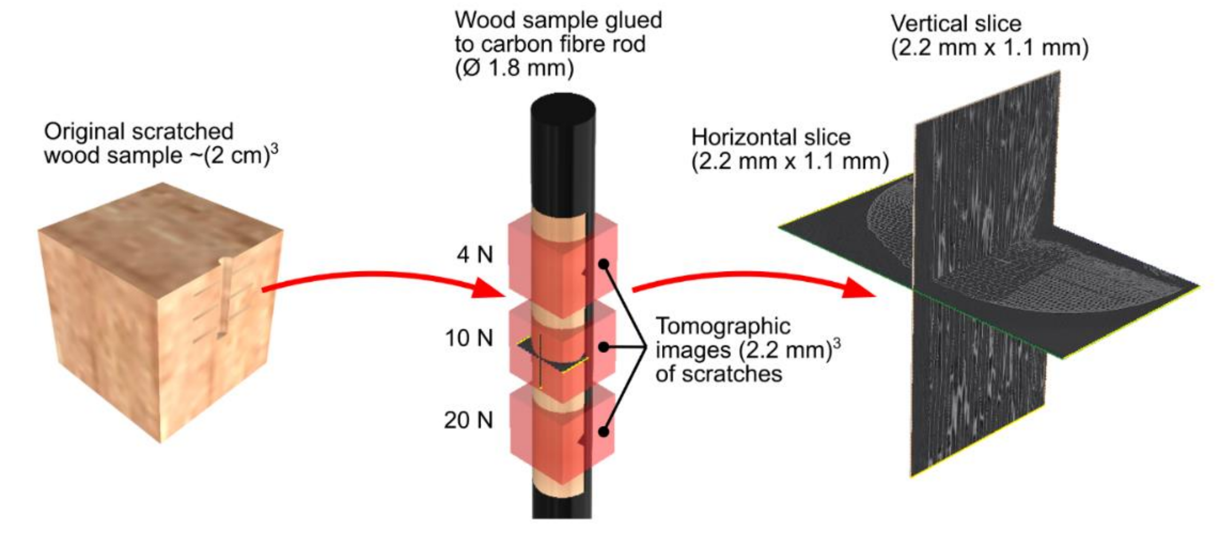

Figure 18 Sample preparation and setup for X-ray tomography. Also shown are examples of horizontal and vertical slices of a three-dimensional tomographic image.

The CT images of wood cells under the scratches in longitudinal direction at different loads are shown in Figure 19 and the measured widths and depths in Table 7. The images for all directions are reported in Appendix II.

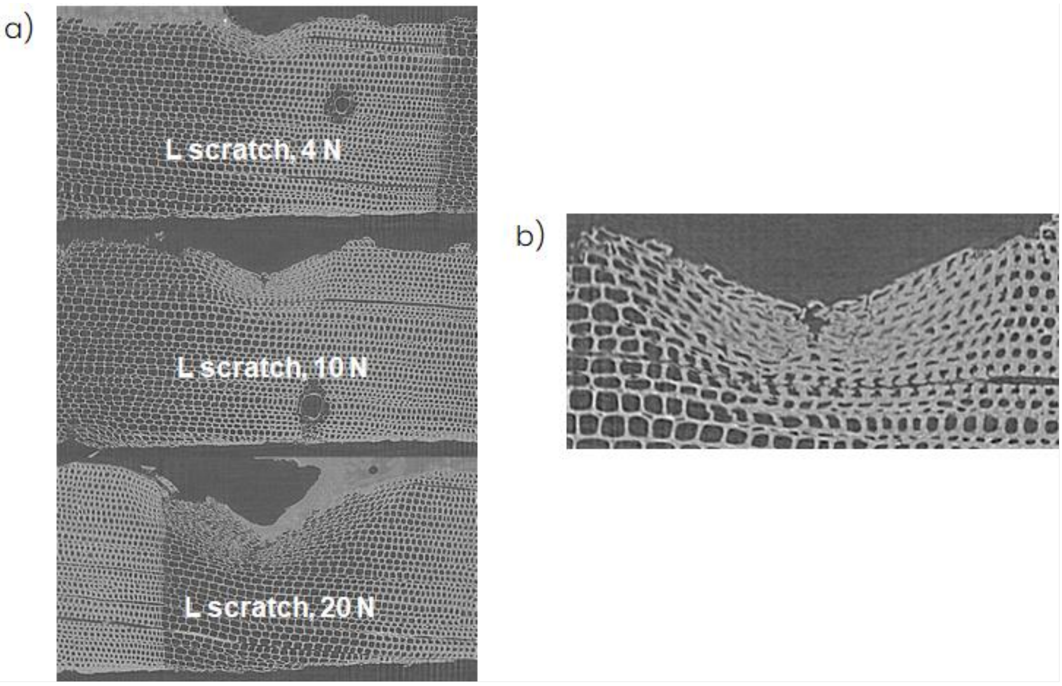

Figure 19 Sample no 75: a) CT tomography images of wood cell wall deformations under longitudinal scratch at different loads. b) zoom of the case under load = 10 N.

Table 7 The depths and widths of scratches in different wood directions and for different scratching forces (sample no 75).

Scratch direction	Scratching force (N)	Cross-sectional area of scratch (μm²)	Maximum depth of scratch (μm)	Average width of scratch (μm)
L	4	31630	92	344
L	10	61006	144	425
L	20	211518	321	659
R	4	22978	61	379
R	10	76184	126	606
R	20	135647	231	587
T	4	13115	40	325
T	10	28222	70	405
T	20	21046	63	335

4.2.2.X-ray Computed Tomography for Timber Components

The CT-tomography for the selected timber components was carried out at VTT with a different device than the one used for the collaboration work about green wood samples with University of Jyväskylä. A summary of the VTT CT facilities is presented in Figure 20.

The imaging work was carried out as follows:

- the RX Solutions Desktom 130 –microtomographic scanner was used;
- 16 μm voxel size was adopted to obtain image of the whole sample;
- the imaging time was around 24 minutes per sample;
- as an output of the imaging, a 3D density map of the image was obtained that can be viewed from any dimensions;
- the locations of scratch grooves were cut to smaller 2D slices for the image analysis.

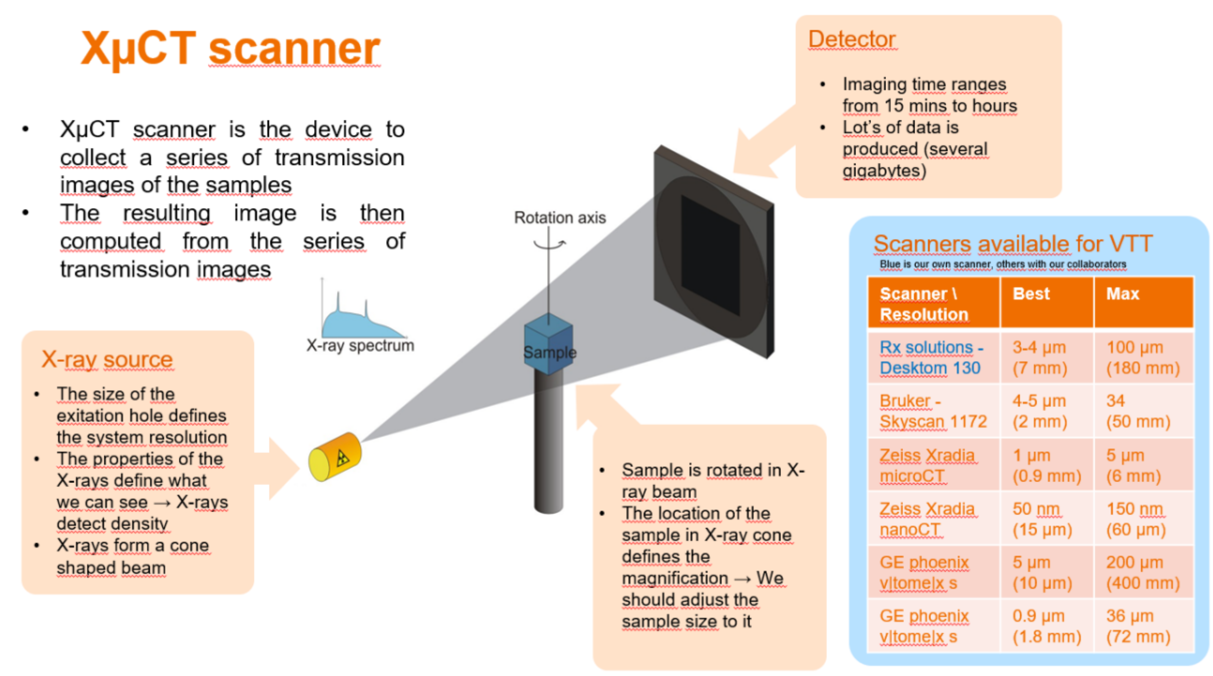

Figure 20 CT tomography facilities at VTT.

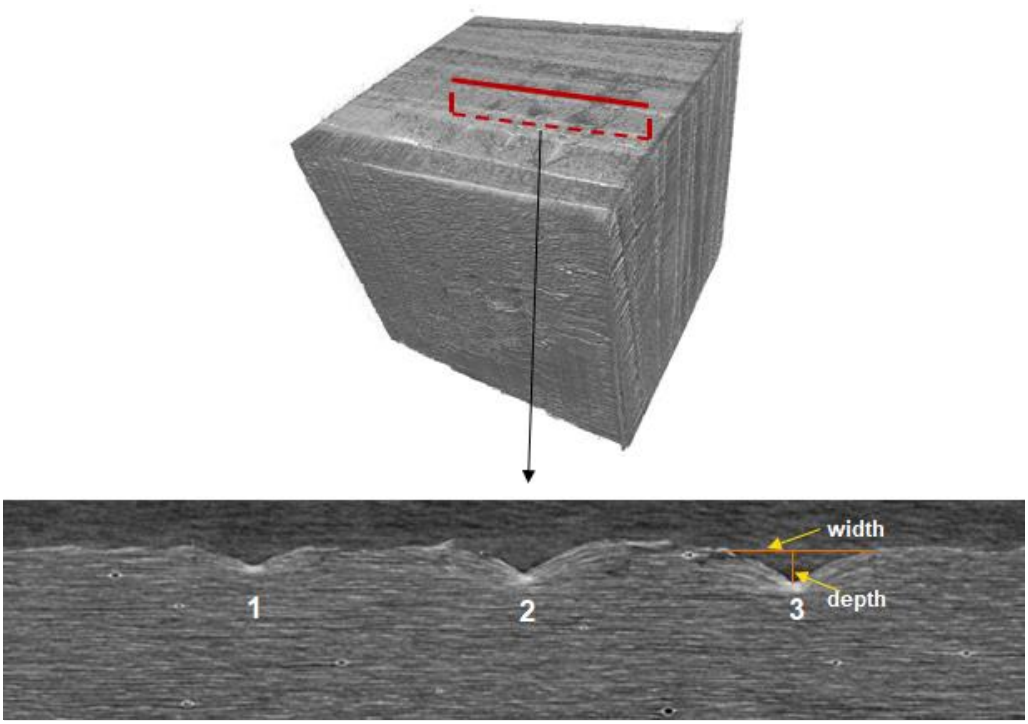

Figure 21 Top: scratches on the 3D images. Bottom: measured width and depth.

The average widths and maximum depths were measured from three scratches per each timber component sample (Figure 21). These values can be used in the mathematical model of scratch resistance (Chapter 5). The CT images for the different samples are reported in Appendix III.

4.3. Results of Scratch Tests

4.3.1. Results of Scratch Tests of Green Wood

The results in format of Excel files can be found in a public data repository available in Zenodo at the following link: https://zenodo.org/record/7993984

The density of the green wood samples was measured after the scratch tests and the scratch test results are presented on the basis of the density of the samples.

Figure 22 represents the friction coefficient values as a function of the sample density in scratch tests that were carried out in R, T, and L directions with different normal loads:

- The linear trendlines are presented to show that friction is decreased as the density of the wood is increasing with all scratching loads.
- The R-squared values related to equation are also presented showing that, yet the trend is visible, the strength of the dependency of the relationship between variables is low.

In Figure 23 the friction coefficient values as function of sample density are presented for radial, tangential and longitudinal scratch directions with 4 N, 10 N, and 20 N normal loads:

- For the radial and tangential directions, the friction coefficient is higher for the higher normal loads.
- For the longitudinal direction, no differences between normal loads were observed.

The normal load represents the indenter load.

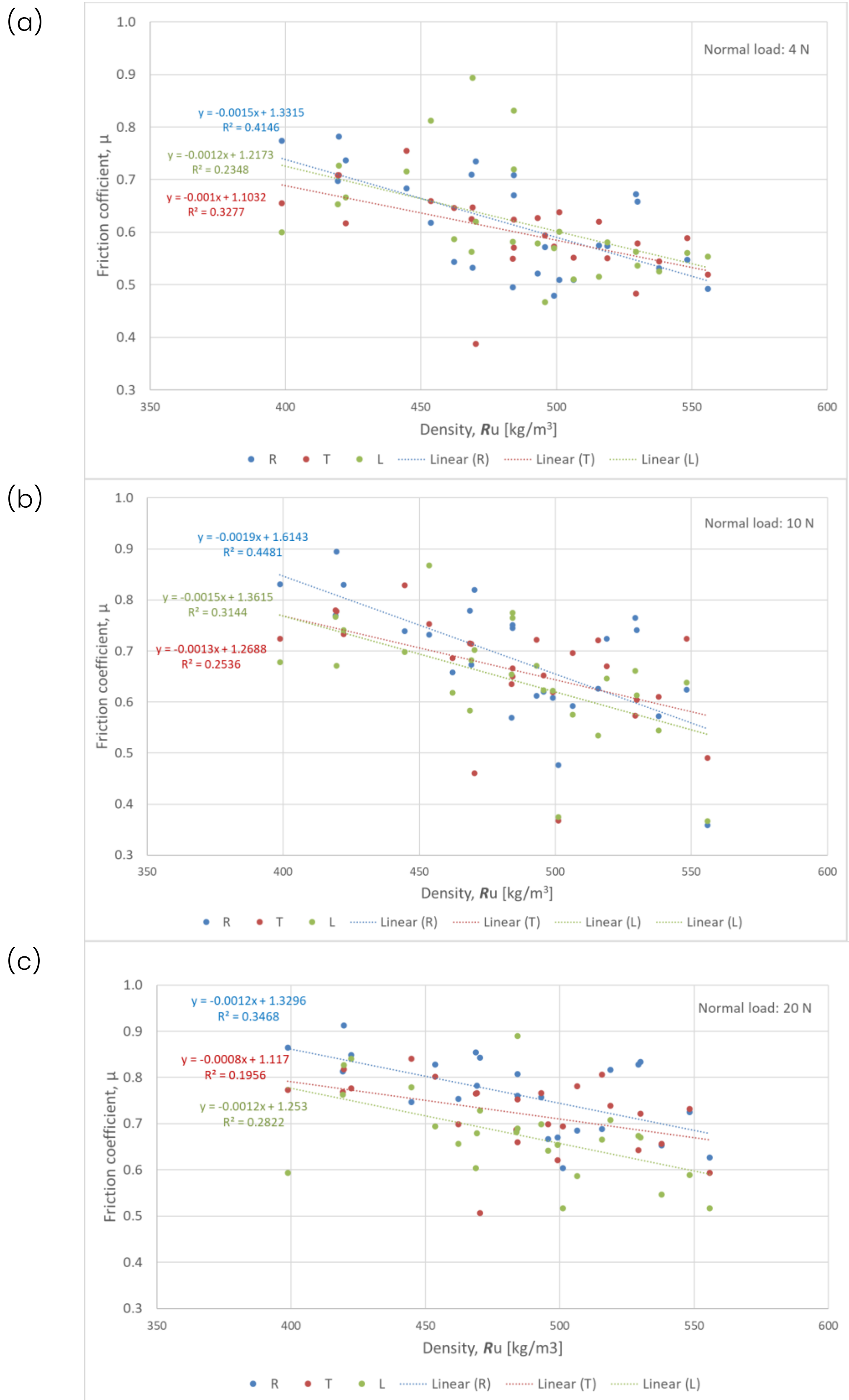

Figure 22 The friction coefficient in scratch tests carried out for GW in R, T, and L directions as function of sample density with normal load of (a) 4 N, (b) 10 N, and (c) 20 N. The linear trendline is presented with the equation and the R-squared values.

(a)

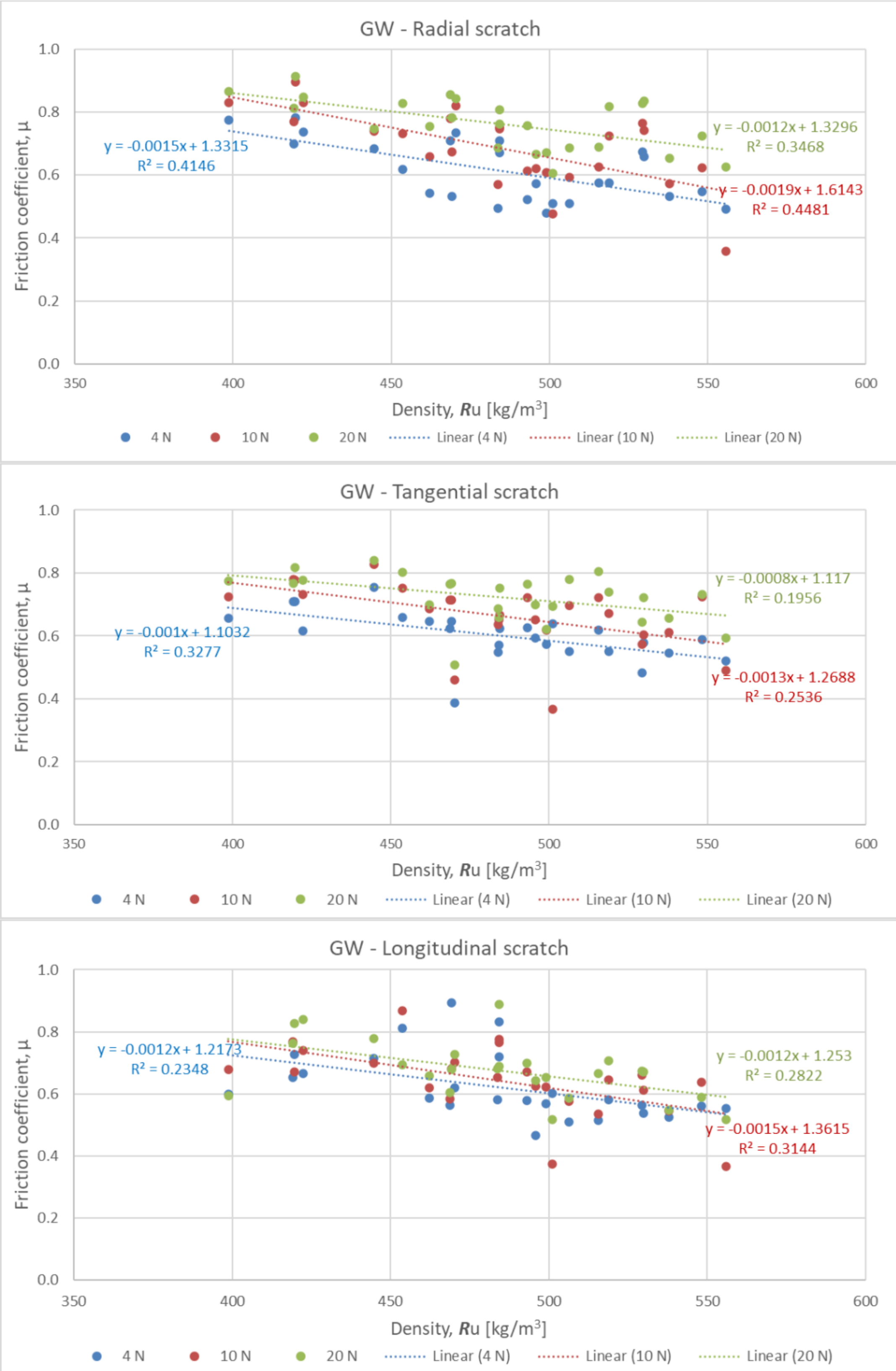

Figure 23 The friction coefficient in scratch tests carried out for GW with 4 N, 10 N, and 20 N normal loads in (a) radial direction, (b) tangential direction, and (c) longitudinal direction as function of sample density. The linear trendline is presented with the equation and the R-squared values.

The influence of normal load is also presented in **Figure 24** for different scratch directions:

- the scratch resistance is increasing with increasing indenter load, especially in the radial direction of wood and less in the longitudinal direction.

To compare the friction of different areas, and therefore the scratch resistance performance of the wood cross section, samples representing the heartwood (samples 58, 59, 64, 65) and sapwood (samples 46, 51, 63, 69) were selected. In this case the heartwood had a lower density (in the range from 399 to 422 kg/m^3) compared to sapwood (in the range from 493 to 556 kg/m^3). The differences in scratch resistance performance are presented in **Figure 25**:

- the higher friction coefficient for the heartwood (lower density) can be clearly observed for all scratch directions and normal loads.

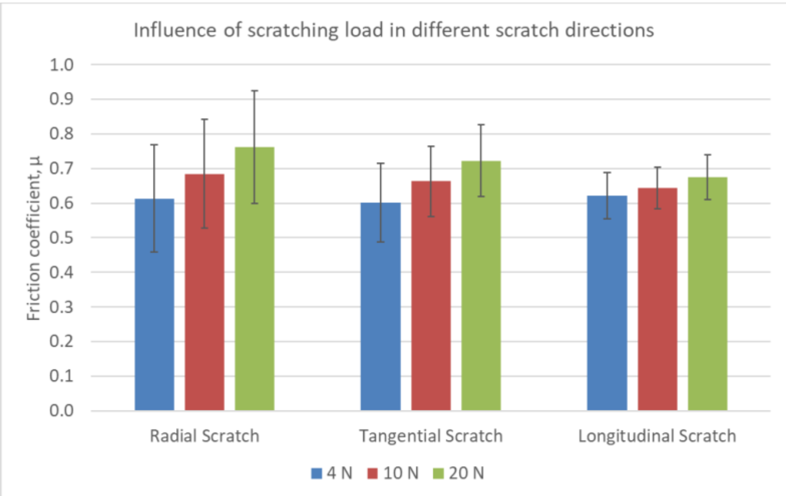

Figure 24 The Influence of normal load in different scratch directions on the friction coefficient.

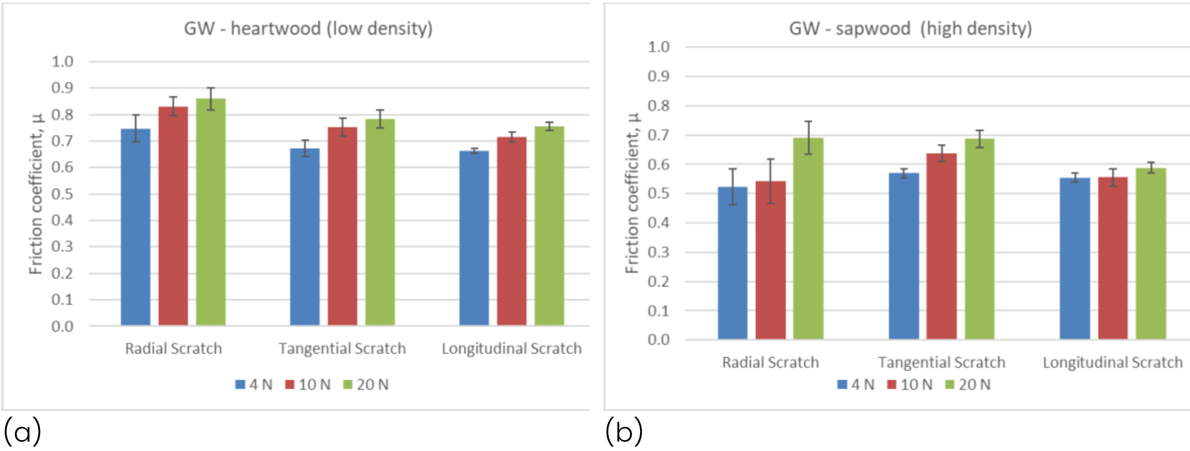

Figure 25 The friction coefficient in scratch testing with normal loads 4 N, 10 N, and 20 N in different scratching directions for (a) heartwood (lower density), and (b) for sapwood (higher density).

4.3.2.Results of Scratch Tests of Timber Components

The results in format of Excel files can be found in a public data repository available in Zenodo at the following link: https://zenodo.org/record/7993984

To investigate the scratch resistance performance of the selected timber components, the friction coefficient values for the samples stored at RH = 65 % are presented in **Figure 26**. The friction coefficient is presented as average values calculated from the complete scratch cycle. The standard deviation represents the fluctuating friction performance as the indenter tip is moving along the surface across the different structural features of the timber sample, such as the tree rings. The scatter is high particularly in the radial direction, since in R direction the indenter is moving against the tree rings with harder and softer areas.

The following phenomena can be observed:

- friction tends to increase as the normal load is increased (the only exceptions can be found for longitudinal scratch direction);
- overall friction performance shows higher friction in radial direction scratches and lowest in longitudinal scratches.

The scratch resistance performance of the samples stored at RH = 85 % are presented in **Figure 27**. Similar trend in the scatter can be found also for these samples. Also, the friction tends to increase while the normal load in increased. Here, exceptions can be found in the longitudinal scratch direction for the samples 10 and 9. The longitudinal scratches provide also in this case lowest friction values.

The influence of the relative humidity on the scratch resistance performance is compared in Figure 28:

- in the radial direction the higher RH increased the friction for all samples;
- in longitudinal direction the friction remains on a similar level for both RH 65 % and 85 % samples;
- in the tangential direction most samples have similar friction, however, samples no 10 and no 5 have higher friction at higher RH;
- the sample 14(M) behaves in a different manner providing lower friction with higher RH. This might be caused by the acrylic water dispersion paint of the tangential surface of the sample.

(a)

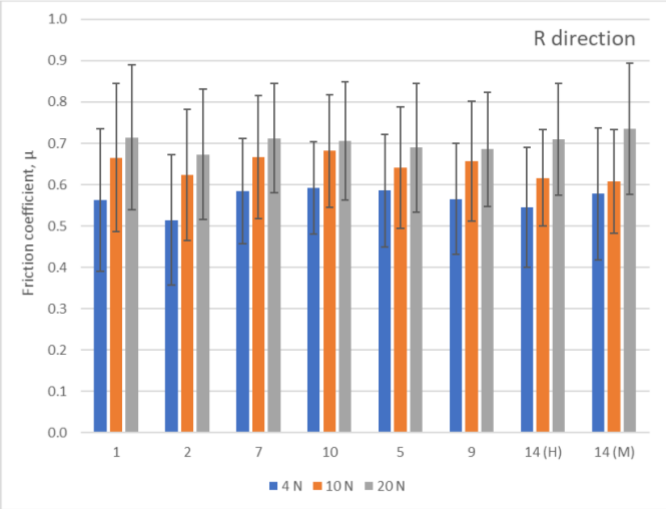

(b)

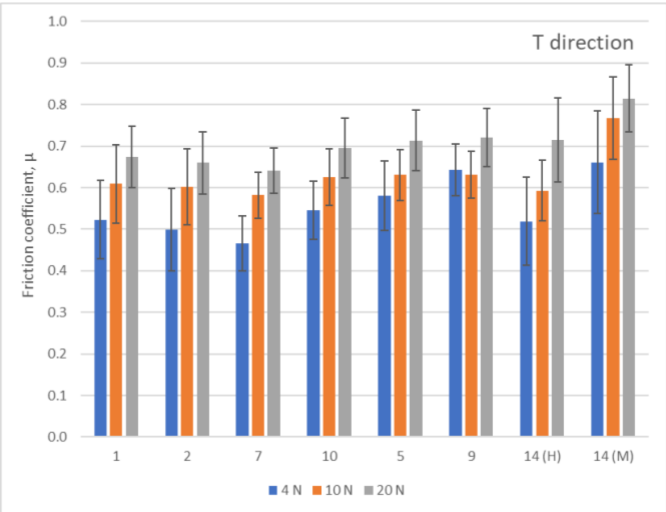

(c)

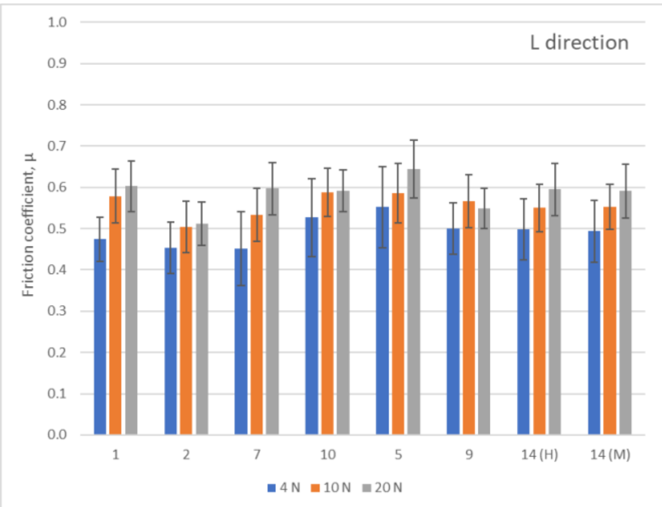

Figure 26 The friction coefficient of timber samples stored in 65 % humidity and scratched with different loads in (a) radial, (b) tangential, (c) and longitudinal direction. No 1 and 7 represent results of one sample, the other results are average values from three samples.

(a)

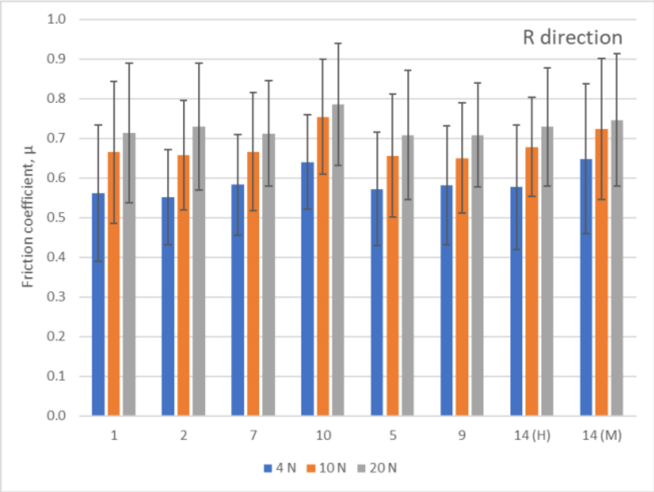

(b)

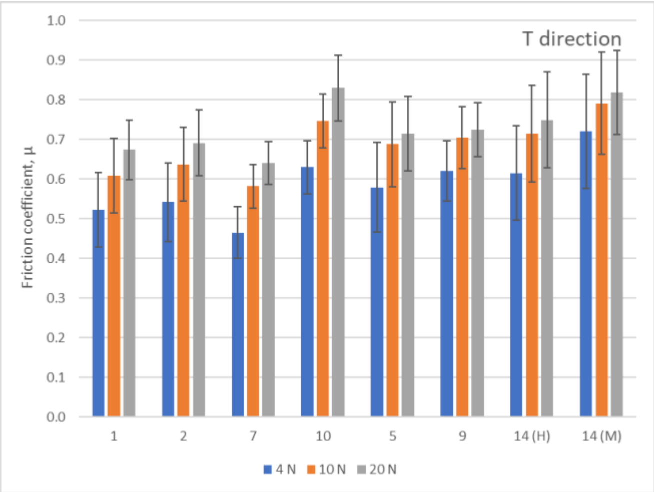

(c)

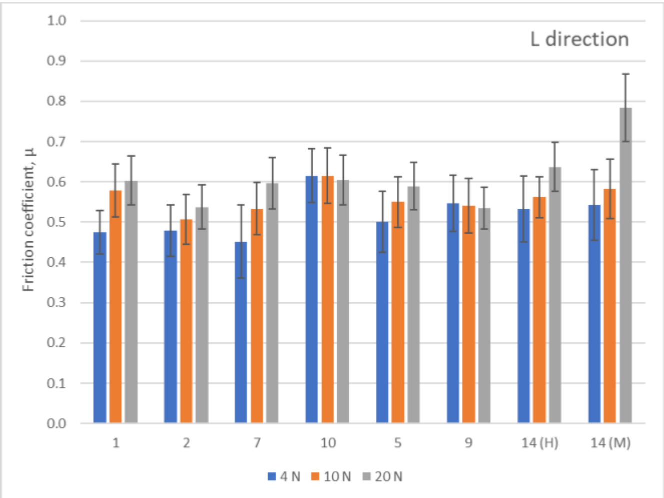

Figure 27 The friction coefficient of timber samples stored in 85 % humidity and scratched with different loads in (a) radial, (b) tangential, (c) and longitudinal direction. No 1 and 7 represent results of one sample, the other results are average values from three samples.

(a)

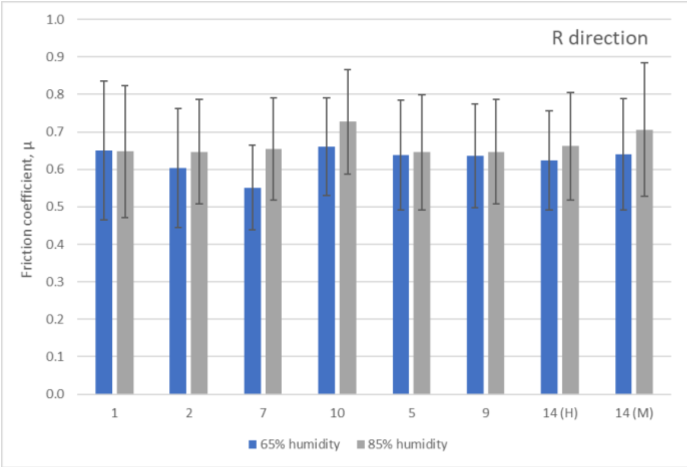

(b)

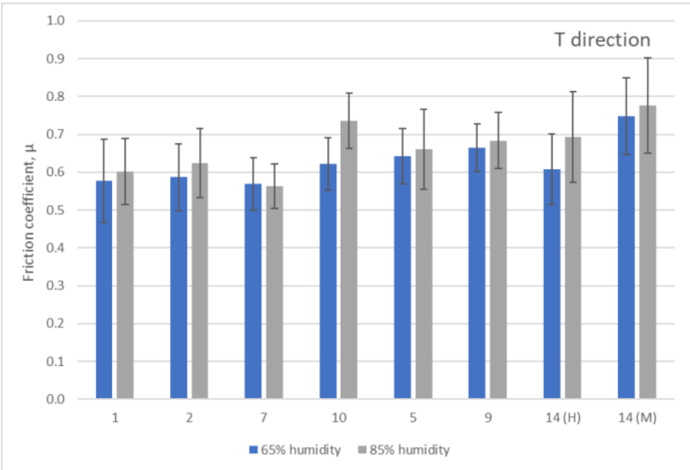

(c)

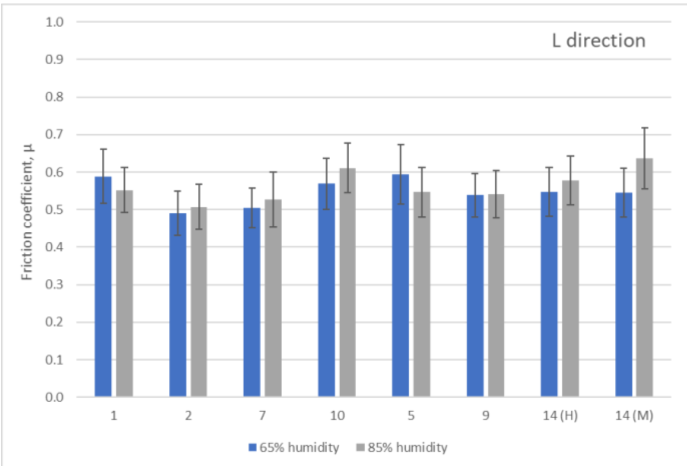

Figure 28 The friction coefficient of timber samples stored in 65 % and 85 % humidity and scratched with different loads in (a) radial, (b) tangential, (c) and longitudinal direction. No 1 and 7 represent results of one sample, the other results are average values from three samples.

5. Scratch Test-based Outcomes

5.1 Correlation Between Scratch Resistance and Cutting Resistance

The scratch resistance or friction force (Ft), representing the force restricting the scratching movement, and the penetration depth (Pd) measured during the scratch testing in radial (R) direction, are presented in Figure 29 for the RH 65% samples and in Figure 30 for the RH 85 % and the following behaviour is found:

- The force resisting the scratch action, that is, the scratch resistance, has a linear dependency on the penetration depth in all wood directions, and for most of the samples the linearity has a reasonably high R^2 values. The increase is steeper for the RH 85% samples compared to RH 65% samples.

Consequently, a correlation between scratch resistance at the material scale and cutting resistance at the wooden component scale can be found. This can be represented by the same type of mathematical equation (Equation 9). In addition, the speed of the cutting blade can be also incorporated by using Equation (10).

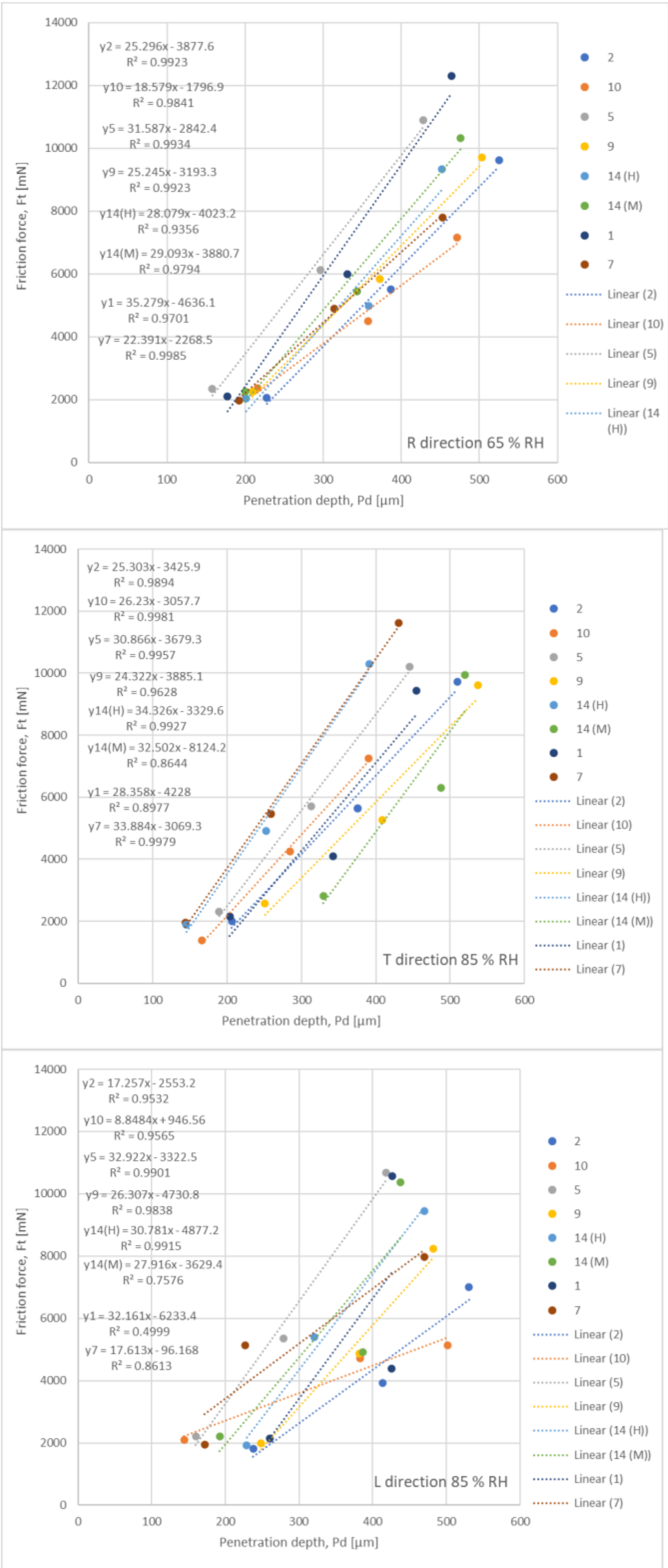

Figure 29 The scratch resistance or friction force (Ft) as a function of penetration depth (Pd) for the timber samples of 65 % humidity in (a) Radial direction, (b) Tangential direction, and (c) Longitudinal direction. The scratches were made in the radial direction. The linear trendlines are presented with the equations and the R-squared values. No 1 and 7 represent results of one sample, the other results are average values from three samples.

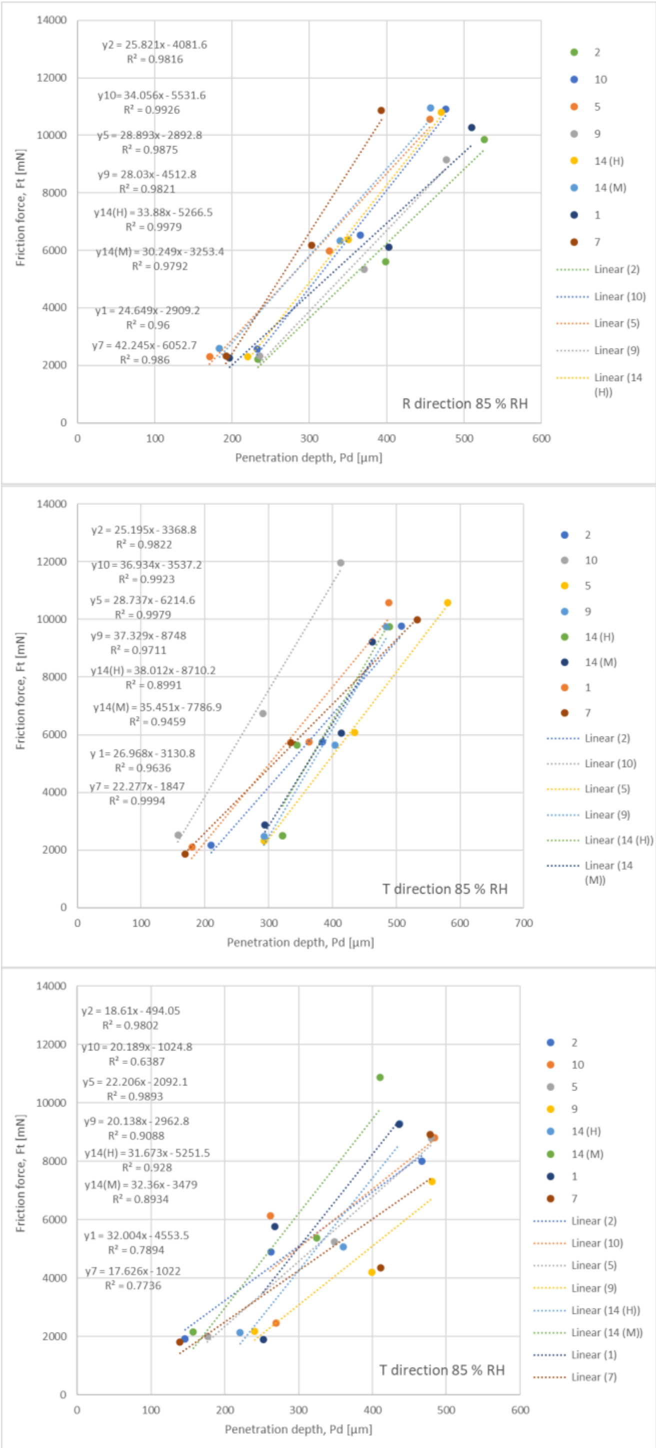

(a)

(b)

(c)

Figure 30 The scratch resistance or friction force (Ft) as a function of penetration depth (Pd) for the timber samples of 85 % humidity in (a) Radial direction, (b) Tangential direction, and (c) Longitudinal direction. The scratches were made in the radial direction. The linear trendlines are presented with the equations and the R-squared values. No 1 and 7 represent results of one sample, the other results are average values from three samples.

Among the other models available in the literature for cutting resistance, a variant of the one proposed by [26] and [27] for wood material can be used to correlate the scratch resistance at the material scale and the cutting resistance at the macroscale of wood and timber components.

Based on the above literature, the preliminary equation for cutting or scratch resistance is the following:

$$F_c\mu = z(\gamma\tau_\gamma) \cdot (bd) + z\alpha R \quad (9)$$

where:

- F_c= cutting force (or indenter force)
- z = number of teeth (of the saw blade); z = 1 in the case of scratch indenter
- μ = friction coefficient
- → $F_c\mu$ = cutting resistance (or scratch resistance, or scratch hardness)
- τ_γ= shear yield strength
- γ = factor (related to shear strain along the shear plane)
- b = cutting width (or scratching width)
- d = cutting depth (or indenter penetration depth)
- → bd =cutting (or scratch) area
- α = factor (related to fracture toughness units)
- R = fracture toughness

Factors γ and α will be assessed in Deliverable D2.2 in conjunction with the HTM models for selected timber components.

In addition, the preliminary equation for cutting or scratch power is written according to [26] as:

$$P_c = F_c v_c + P_{ac} \quad (10)$$

where:

- F_c= cutting force (or indenter force)
- v_c = cutting speed
- P_{ac} = variation of chip acceleration power defined as

- $P_{ac} = \dot{m}v_c^2$ (11)

where $\dot{m}$ is the mass of wood (chips) evacuated in a certain period of time at a certain cutting speed, and defined as

- $\dot{m} = Hbv_p\rho$ (12)

where:

- H = wood thickness
- b = cutting width
- v_p = speed of penetration
- ρ = wood density

Equations (9) and (10) can be easily implemented in the same ***end-user digital tool*** where the results of HTM analyses will be collected within working package WP2. For instance, this tool can be the ***VTT Modelling Factory environment***. This issue will be assessed in D2.2.

The model allows a linear interpolation of the experimental data providing important material properties:

- A measure of the **shear yield strength**, that is the slope of the linear regression curve, which is a measure of the ***shear failure risk*** in the wooden components under cutting or under loads causing shear failure, for example close to the supports of beams.
- A measure of the **fracture toughness**, that is the intercept of the linear regression curve on the Y-axis, which is a measure of the ***crack propagation risk*** under cutting or other loads causing shear failure.

This is an important scientific finding to be further explored for publication in peer-reviewed papers.

From a practical point of view, the upscaling from the material scale to the macroscale of wooden components is possible considering the average values of b and d for the material scratching and the macroscale cutting, as well as the initial cracking width and depth in wooden components under mechanical loads.

5.1. Information to Industry

The scratch tests are a simple approach to get important information during industrial operations such as:

- cutting of wood in sawmills to produce lumbers;
- cutting of timber components before the installation in production or on site;
- monitoring of shear failures in timber components during their service life.

Summarizing the results from the previous sections and considering the correlation between scratch resistance at the material scale and cutting resistance at the wooden component scale, the information of industrial interest is listed below.

1. Information from scratch tests on green pine wood:
   - The cutting resistance decreases almost linearly as the density of the wood increases under various levels of cutting loads.
   - The cutting resistance increases with increasing cutting load, especially in the radial direction of wood and less in the longitudinal direction.
   - The cutting resistance is higher for lower density of wood, and this can be observed for all wood directions and cutting loads.
   - The levels of fracture toughness and shear yield strength of the wood can be evaluated by upscaling the scratch test results.
2. Information from scratch tests on timber components:
   - The cutting resistance tends to increase as the cutting load increases (the only exceptions can be found for longitudinal wood direction).
   - The overall cutting resistance performance is higher in radial direction of wood and lower in longitudinal direction.
   - In the radial direction of wood, higher air RH and wood moisture content (RH=85%, MC=18%) increase the cutting resistance of the wood.
   - In the longitudinal direction of wood, the cutting resistance is almost the same at both RH 65 % (MC=12%) and RH 85 % (MC=18%).
   - In the tangential direction of wood, most wooden components have similar cutting resistance.

- Samples coated with acrylic water dispersion paint show lower cutting resistance with higher RH.

5.1.1. Practical use of scratch test results in cutting operations

The results from scratch tests at the material scale can be upscaled to the structural scale of the following machines:

- saw blade machines, such as sash gang saws and band sawing machines.

Concerning the cutting operations in sawmills and before installation in buildings, to upscale the scratch test results, the following parameters are needed from the industrial companies:

- wood thickness
- wood density
- wood MC
- cutting direction
- number and dimensions of saw blade teeth
- saw blade width
- cutting force
- cutting speed

The levels of fracture toughness and shear yield strength of the wood evaluated by upscaling the scratch test results will also serve to evaluate the shear performance of wooden components under their service life.

It has to be noticed that knots in wood are not taken into account in the models, however, to evaluate the fracture toughness and shear yield strength, usually samples free of knots are tested.

6. Conclusions

Deliverable 2.1 collects the input data on material properties and environmental conditions to be used in the HTM analyses to be presented in Deliverable D2.2. The results of D2.2 will then be used for the work to be carried out in Task T2.6 about predictive maintenance and to support the long term SHM investigations of Use case UC3.2.

In D2.1, the main hygro-thermal properties and the related models, to be used in D2.2, are explained and listed. Only some of the mechanical properties are listed along with a summary of the related models. For most of the mechanical properties, the reader is referred to the relevant literature.

This deliverable presents a large number of new results on scratch tests of green wood and timber components. The results are of great scientific value since there is a lack of literature on scratch tests of wood.

From the industrial point of view, the new scratch test results provide important information on the effects of wood directions, density and MC under cutting-type loads on relevant material properties to be monitored during the whole value chain of wood components, from their production to the end of their service life. Mathematical equations for the cutting resistance and the cutting power allow to correlate the scratch tests results to the real cutting operations. The related information is useful for sawmills, production and construction companies, as well as the monitoring activities to be carried out before and during the installation of wooden components in products and buildings. The related models will be also used in connection with the HTM analyses to be carried out for D2.2.

7. References

[1] S. Thelandersson *et al.*, "Service life of wood in outdoor above ground applications - engineering design guideline," *Background document. Report TVBK-3061. Div. of Structural Engineering. Lund University*. https://www.lunduniversity.lu.se/lup/publication/5489b12f-f950-4cd5-9555-d4cf5786da1a (accessed May 26, 2023).

[2] J. Song *et al.*, "Processing bulk natural wood into a high-performance structural material," *Nature*, vol. 554, no. 7691, 2018, doi: 10.1038/nature25476.

[3] J. Arfvidsson *et al.*, *WOOD IN CARBON EFFICIENT CONSTRUCTION - Tools, methods and applications*. European Confederation of Woodworking Industries (CEI-BOIS), 2013. Accessed: May 26, 2023. [Online]. Available: https://research.aalto.fi/en/publications/wood-in-carbon-efficient-construction-tools-methods-and-applicati

[4] M. Fragiacomo, S. Fortino, D. Tononi, I. Usardi, and T. Toratti, "Moisture-induced stresses perpendicular to grain in cross-sections of timber members exposed to different climates," *Eng Struct*, vol. 33, no. 11, 2011, doi: 10.1016/j.engstruct.2011.06.018.

[5] C. Brischke and L. Meyer-Veltrup, "Modelling timber decay caused by brown rot fungi," *Materials and Structures/Materiaux et Constructions*, vol. 49, no. 8, 2016, doi: 10.1617/s11527-015-0719-y.

[6] J. Van den Bulcke, I. De Windt, N. Defoirdt, J. De Smet, and J. Van Acker, "Moisture dynamics and fungal susceptibility of plywood," *Int Biodeterior Biodegradation*, vol. 65, no. 5, 2011, doi: 10.1016/j.ibiod.2010.12.015.

[7] O. Schmidt, *Wood and tree fungi: Biology, damage, protection, and use*. Berlin: Springer, 2006. doi: 10.1007/3-540-32139-X.

[8] APAwood Europe, "EN 350: 2016 (updated) Durability of wood and wood-based products - Testing and classification of the durability to biological agents of wood and wood-based materials," *The Engineered Wood Association* , 2016. https://standards.iteh.ai/catalog/standards/cen/b02d18a7

-87ce-4a20-84c7-c0de641a2780/en-350-2016 (accessed May 26, 2023).

[9] S. Fortino, P. Hradil, A. Genoese, A. Genoese, and A. Pousette, "Numerical hygro-thermal analysis of coated wooden bridge members exposed to Northern European climates," *Constr Build Mater*, vol. 208, pp. 492–505, May 2019, doi: 10.1016/J.CONBUILDMAT.2019.03.012.

[10] S. Franke, B. Franke, and A. M. Harte, "Failure modes and reinforcement techniques for timber beams – State of the art.," *Constr Build Mater*, vol. 97, no. 2–13, 2015.

[11] S. Fortino, F. Mirianon, and T. Toratti, "A 3D moisture-stress FEM analysis for time dependent problems in timber structures," *Mech Time Depend Mater*, vol. 13, no. 4, 2009, doi: 10.1007/s11043-009-9103-z.

[12] H.-L. Frandsen, "Modelling of moisture transport in wood – State of the Art and Analytic Discussion," Aalborg University, Aalborg, 2005.

[13] L.-O. Nilsson, "Moisture transport properties of wood and wood-based boards – an inventory and analysis of knowledge and required knowledge (in Swedish)," Göteborg, Sweden, 1988.

[14] J. Sjödin, "Steel-to-timber dowel joints : influence of moisture induced stresses," 2006.

[15] A. Hanhijärvi, "Modelling of creep deformation mechanisms in wood," *VTT Publications*, no. 231, 1996.

[16] E. E. Thybring, M. Kymäläinen, and L. Rautkari, "Experimental techniques for characterising water in wood covering the range from dry to fully water-saturated," *Wood Sci Technol*, vol. 52, no. 2, 2018, doi: 10.1007/s00226-017-0977-7.

[17] H.-L. Frandsen, "Selected Constitutive Models for Simulating the Hygromechanical Response of Wood," Dissertation no. 10, ISSN: 1901-7294, 2007, Aalborg University, Aalborg, 2007. Accessed: May 26, 2023. [Online]. Available: https://vbn.aau.dk/en/publications/selected-constitutive-models-for-simulating-the-hygromechanical-r

[18] S. Fortino, P. Hradil, and G. Metelli, "Moisture-induced stresses in large glulam beams. Case study: Vihantasalmi Bridge,"

Wood Mater Sci Eng, vol. 14, no. 5, 2019, doi: 10.1080/17480272.2019.1638828.

[19] S. Avramidis, "Evaluation of 'three-variable' models for the prediction of equilibrium moisture content in wood," *Wood Sci Technol*, vol. 23, no. 3, 1989, doi: 10.1007/BF00367738.

[20] A. A. Chiniforush, M. Gharib, and A. Akbarnezhad, "A Unified Moisture Sorption–Desorption Isotherm for Engineered Wood," *Journal of Materials in Civil Engineering*, vol. 33, no. 11, 2021, doi: 10.1061/(asce)mt.1943-5533.0003932.

[21] "EN ISO 7783-1:1999 - Paints and varnishes - Determination of water-vapour transmission rate - Part." https://standards.iteh.ai/catalog/standards/cen/1b7d1c5b-6aec-469a-8900-718313febdfa/en-iso-7783-1-1999 (accessed May 26, 2023).

[22] S. Koponen, "Lämpö- ja kosteusoloiltaan miellyttävä puutalo, vaihe 2, TKK-TRT osatutkimus, Raportti 1," 2002.

[23] S. Svensson and T. Toratti, "Mechanical response of wood perpendicular to grain when subjected to changes of humidity," *Wood Sci Technol*, vol. 36, no. 2, 2002, doi: 10.1007/s00226-001-0130-4.

[24] Jönsson J., "Moisture Induced Stresses in Timber Structures | Lund University," Technical Report TVBK-1031, Dissertation, Lund University of Technology., 2005. Accessed: May 26, 2023. [Online]. Available: https://www.lunduniversity.lu.se/lup/publication/68796182-697c-4280-a767-35664a69439d

[25] S. Fortino, J. Metsäjoki, H. Ronkainen, I. Bjurhager, S. Heinemann, and L. I. Salminen, "Scratch resistance of PEG-impregnated green wood: a method for evaluation of swollen wood properties," *Wood Sci Technol*, vol. 54, no. 3, 2020, doi: 10.1007/s00226-020-01179-0.

[26] K. A. Orlowski, T. Ochrymiuk, A. Atkins, and D. Chuchala, "Application of fracture mechanics for energetic effects predictions while wood sawing," *Wood Sci Technol*, vol. 47, no. 5, 2013, doi: 10.1007/s00226-013-0551-x.

[27] L. Hlásková, K. A. Orlowski, Z. Kopecký, M. Sviták, and T. Ochrymiuk, "Fracture toughness and shear yield strength determination for two selected species of central European

Provenance," *BioResources*, vol. 13, no. 3. 2018. doi: 10.15376/biores.13.3.6171-6186.

8. Appendix I

From the review carried out by [22]. The references can be found in that paper.

Material/paint type and substrate	Test method: Dry cup (D)/ Wet (W) cup	Resistance (m^2 s Pa/kg)	Permeance (kg/m^2 s Pa)	Substrate	Reference
Pressure polymer paint, Novaplast 2	W	2,3E+07	4,3E-08		Tikkurila (2002)
Akrylic copolymer paint, Siroplast 20	W	3,7E+08	2,7E-09	permeable film	Tikkurila (2002)
½" Gypsum wall board (=GWB), no paint	D	4,2...4,6 E+8	2,2...2,4 E-9		Gelin L. https://www.jm.com/
Water-based acrylic varnish Paneeli-Ässä	W	5,5E+08	1,8E-09	permeable film	Tikkurila (2002)
Pressure polymer paint, Novaplast 20	W	5,7E+08	1,7E-09	permeable film	Tikkurila (2002)
Pressure polymer paint, Novaplast 7	W	5,8E+08	1,7E-09	permeable film	Tikkurila (2002)
Acryl latex paint 50 µm, no primer	RH 90%	6,8E+08	1,5E-09		Nevander (1994)
Acryl latex paint, Harmony	W	7,9E+08	1,3E-09	permeable film	Tikkurila (2002)
Acrylic latex paint, Remontti-Ässä	W	8,0E+08	1,3E-09	permeable film	Tikkurila (2002)

Interior latex paint system = primer +finish coat	D/W	1,0E+09	1,0E+09	gypsum wallboard	Zarr et al. (1995)
½" GWB with JM Textra + 2 coats flat paint*	D	1,1E+09	9,4E-10	gypsum wallboard	Gelin L. https://www.jm.com/
½" GWB + latex Primer	D	1,94...2,5E+09	4,0...5,1E-10	gypsum wallboard	Gelin L. https://www.jm.com/
Acryl latex paint 50 µm, no primer	RH 60%	2,7E+09	3,7E-10		Nevander (1994)
Alkyd oil paint 50 µm, no primer	RH 90%	3,4E+09	3,0E-10		Nevander (1994)
½" GWB with JM Textra (glass textile wallcovering) + 2 coats satin paint	D	3,6E+09	2,8E-10	gypsum wallboard	Gelin L. https://www.jm.com/
Water-based epoxy, Akvacoat 100"new"	W	3,9E+09	2,6E-10	permeable film	Tikkurila (2002)
½" GWB with JM Textra, latex primer + 2 coats satin paint*	D	6,7E+09	1,5E-10	gypsum wallboard	Gelin L. https://www.jm.com/
Alkyd paint, Pesto	W	7,8E+09	1,3E-10	permeable film	Tikkurila (2002)
Alkyd oil paint 50 µm, no primer	RH 60%	1,0E+10	9,9E-11		Nevander (1994)
Chlorinated rubber paint	W	2,7E+10	3,7E-11	permeable film	Tikkurila (2002)

TEMACOAT RM40					
Moisture barrier, Lujamethod ks+2xLuja pk	W	3,4E+10	3,0E-11	permeable film	Tikkurila (2002)
½" GWB + Vinyl Wallcovering	D	2,2...35 E+10	2,9E-12	gypsum wallboard	Gelin L.

9. Appendix II

Tomography images of scratches in green wood (Sample no 75)

Sample	Image - horizontal	Image - vertical
Longitudinal direction	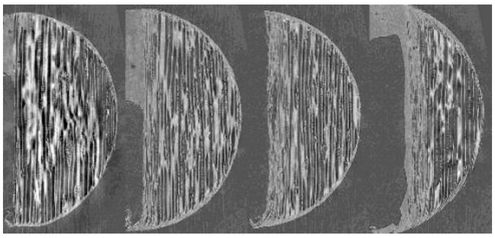	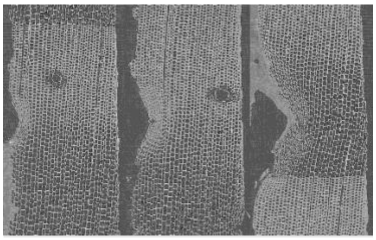
Radial direction	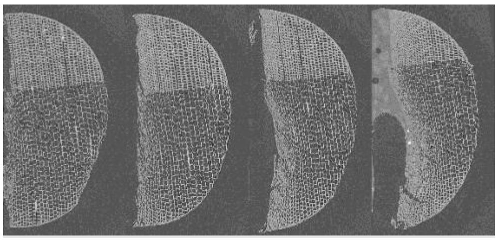	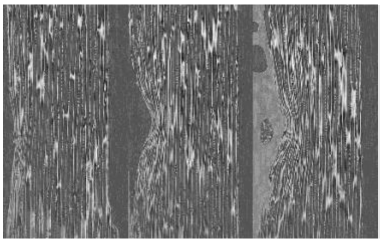
Tangential direction	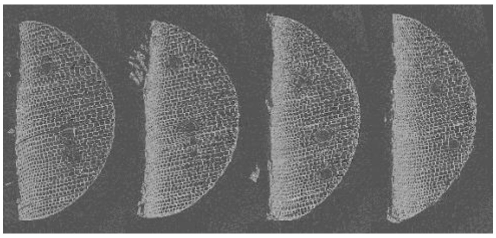	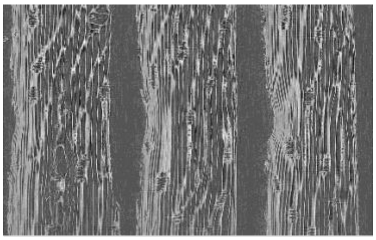

10. Appendix III

Tomography images from timber components referred to 2 sets of samples (Set 1 with MC=12% and Set 2 with MC=18%) taken from selected samples (codes from Table 6):

Sample code	Images from Set 1 (MC 12%)	Images from Set 2 (MC 14%)
1	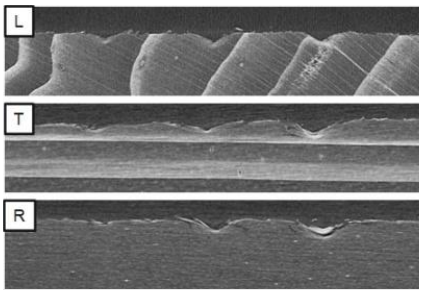	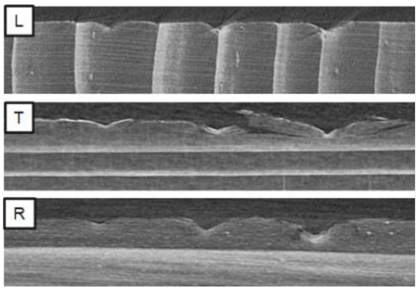
2	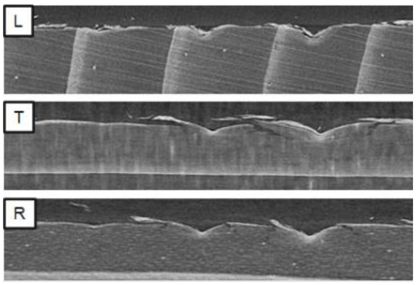	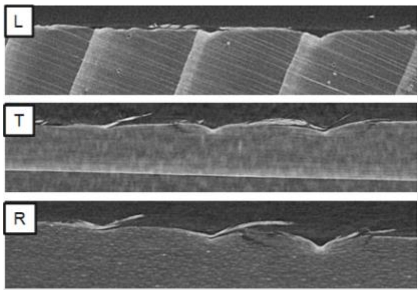
5	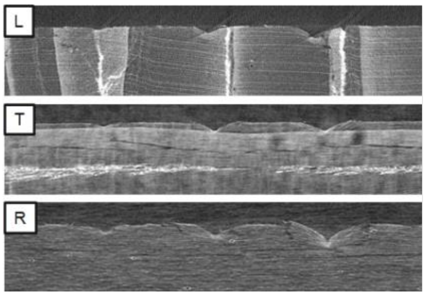	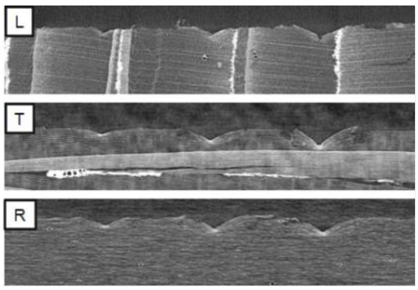

7	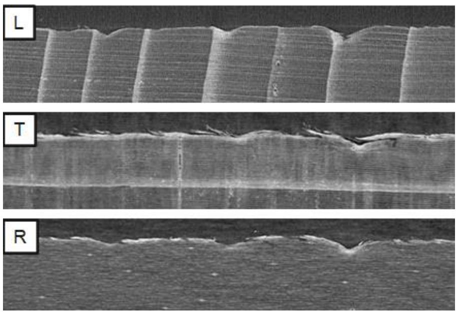	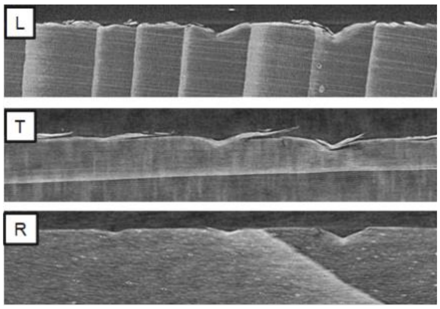
9	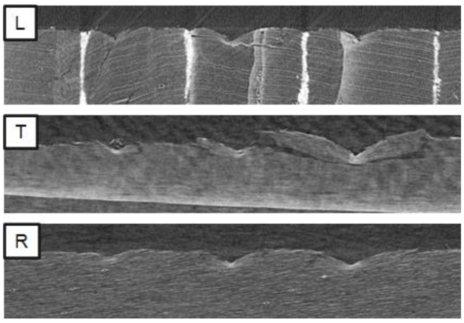	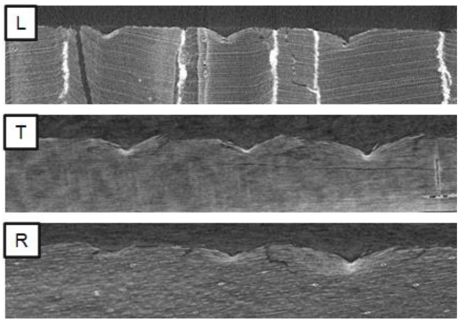
10	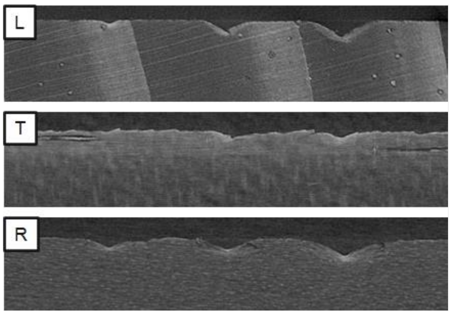	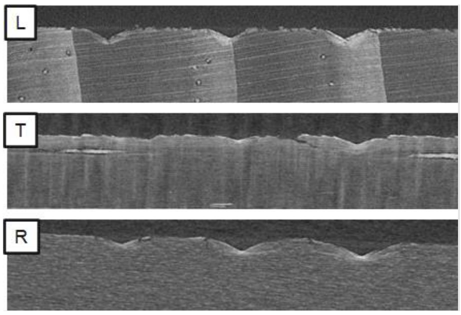
14(H)	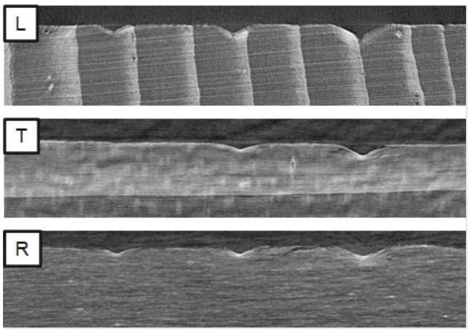	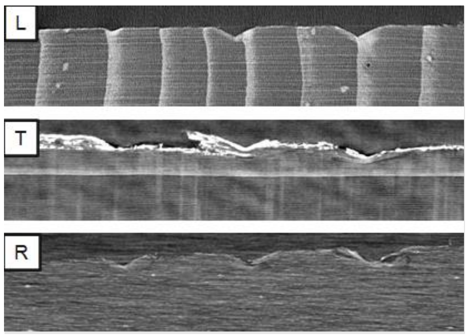

14(M)